AD/COM

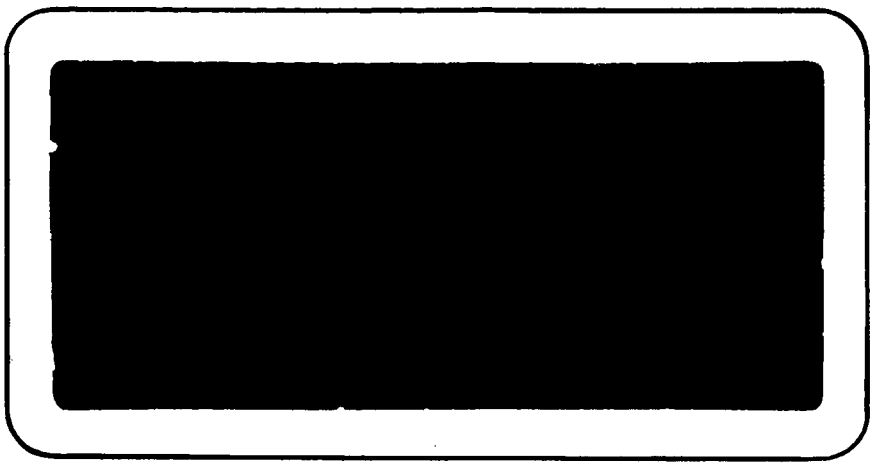

ADCOM, INC.
808 Memorial Drive
Cambridge, Mass. 02139
868-1000

ADVANCED COMMUNICATION RESEARCH AND DEVELOPMENT

SYSTEM FOR THE MEASUREMENT OF OSCILLATOR INSTABILITY

31 October 1965

Prepared for

National Aeronautics and Space Administration
George C. Marshall Space Flight Center
Huntsville, Alabama

under

Contract No. NAS 8-11228
Task Order Nos. ASTR-AD-12 and ASTR-AD-13

Authorship

Ahmad F. Ghais
Richard N. Lincoln
Southard Lippincott
Peter A. Olendzenski
Richard W. Porter

Approved by Steven M. Sussman
Director of Research

Submitted by

ADCOM, Inc.
808 Memorial Drive
Cambridge, Massachusetts 02139

TABLE OF CONTENTS

LIST OF ILLUSTRATIONS

LIST OF ILLUSTRATIONS (Cont.)

1. INTRODUCTION

1.1 Purpose and Scope of Report

This report documents the results of a study and laboratory development effort authorized by two task orders under the subject contract. The description of work in Task Order No. ASTR-AD-12 reads as follows:

> The contractor shall perform the work necessary to devise, test and evaluate a breadboard model of a new technique for measuring the frequency instability of high precision oscillators, such as a hydrogen maser. The objective is to demonstrate the feasibility of a coherent detection measurement technique which suitably expresses the spectral characteristics of a CW signal in a manner that characterizes the frequency instability of an oscillator in a useful way by measuring the power density spectrum of the frequency or phase fluctuations of the oscillator output signal.
>
> The measurement system shall be applicable to the: evaluation of the frequency stability of the maser; evaluation of the frequency stability of crystal oscillators to be used in 1 MHz synthesizers; evaluation of the degradation of signals processed by synthesizer components (multipliers, mixers, etc.); evaluation of synthesized 1 MHz signals; and evaluation of future high precision oscillators.
>
> Seeing that other known and used methods of characterizing and measuring frequency instability are inadequate for the tasks listed above, the new measurement system should fill an important current need. The measurement of the power spectral density of frequency instability is the only method capable of providing sufficient data for the performance of the above tasks.
>
> The complete task shall include the following subtasks:
>
> a. Automatic Detection Loop Development - Design, specify and procure loop components including motor, geartrain, resolver and dc amplifier. Construct phase detector and loop filter. Utilizing a stable 1 MHz crystal source and a special low frequency spectrum analyzer, test and determine performance of the loop including, but not limited to: detection sensitivity, closed-loop filtering parameters, lock-in range, and distortion.

b. Predetection Error Multiplication Development - The object here is to design and develop circuits that are suitable for error multiplication and hence increase the sensitivity of the above loop system. The circuits must be designed to accept the 1 MHz signals contemplated in NASA's application. The critical elements of the error multiplication system are the first multiplier stages. Utilizing the automatic detection loop as a measurement instrument, optimize these multipliers for minimum signal degradation and implement the system for minimum undesired cross coupling and feedback.

c. System Integration, Test and Evaluation - Integrate system into a self-contained rack-mounted breadboard configuration. Devise techniques for absolute calibration of output indications in terms of input frequency and phase fluctuations and systems parameters. Determine overall detection sensitivity as a function of rate of frequency fluctuations.

The description of work in Task Order No. ASTR-AD-13 reads as follows:

> Develop a unified method of measuring and specifying the characteristics of oscillator spectra using the measurement technique developed on Task No. ASTR-AD-12. The objective is to derive methods to prescribe quantitatively and measure effects of a number of signal processing techniques (such as mixers, frequency multipliers and dividers, etc.) necessary for the generation of an ultra-stable 1 MHz signal from ultra-stable sources in the region above 10 GHz.

Since the above descriptions of work are closely interrelated, it was felt appropriate, in the interest of continuity and clarity, to prepare a unified report covering both tasks.

The scope of our work on Task ASTR-AD-12 encompassed the effort required to devise, test and evaluate a new technique for measuring the frequency instability of high precision oscillators. The major problem here was to design implement, test and evaluate a breadboard system that was shown to

evaluate the mean-square spectral density of short-term phase fluctuation and the long term frequency fluctuations of two stable sources. The work involved primarily the development of automatic detection loop circuits, predetection error multiplication circuits and the solution of the system interface problems. The end result of this task was a laboratory breadboard that demonstrated the feasibility and usefulness of the new technique in practical application.

The scope of our work on Task ASTR-AD-13 encompassed a reevaluation of existing methods and recommendation of new criteria and methods for specifying and measuring the performance characteristics in the light of the new capability demonstrated by the Task 12 breadboard system. The objective of this task is to devise operationally-suitable methods and procedures for the Task ASTR-AD-12 system that will yield the data required for evaluating the performance characteristics of ultra-stable oscillators and related signal processing techniques.

1.2 The Measurement Strategy

Previous work by ADCOM, Inc., under Contract No. NAS8-11228 has shown the need for a new approach to oscillator instability, with a requisite new characterization of the signal properties of oscillator output and a new measurement concept.[1-4] Basically, this work showed that the performance of an oscillator in a system sensitive to only the zero-crossing or phase stability of an oscillator signal as a first-order effect is best described by the mean-square spectral density of the real-time frequency deviation random process, $S_{\dot{\phi}}(\omega)$.

The oscillator signal is described as

$$e(t) = a(t) \cos (2\pi \bar{f} t + \phi(t)), \qquad (1)$$

where $\bar{f}$ is the long term frequency of the oscillation, averaged over all time of interest in any applications such that it can be considered to be constant, and

$\phi(t)$ is a random process representing the deviation in phase of the oscillation from the perfect ramp $2\pi \bar{f}\, t$. Denoting the argument of the cosine function in Eq. (1) as

$$\theta(t) = 2\pi \bar{f}\, t + \phi(t), \tag{2}$$

and differentiating once with respect to time, we see that

$$\dot{\theta}(t) = 2\pi \bar{f} + \dot{\phi}(t) \tag{3}$$

Now $\dot{\theta}(t)$ can be seen to be a nonzero-mean random process, which is split into its average and deviant parts in Eq. (3), such that $\dot{\phi}(t)$ is a zero-mean random process and

$$\dot{\phi}(t) = \dot{\theta}(t) - \bar{\dot{\theta}}(t) \tag{4}$$

It is the phase process, $\phi(t)$, whose spectral density, $S_{\phi}(\omega)$, serves as the best description of oscillator instability in zero-crossing sensitive systems.

In that

$$\dot{\phi}(t) = \frac{d\phi(t)}{dt}\ , \tag{5}$$

$$S_{\dot{\phi}}(\omega) = \omega^2 S_{\phi}(\omega)\ , \tag{6}$$

either spectral density is an adequate description of the oscillator signal, and either can be used as a basic measurement output to be converted to the other.

Reference 1 also shows that the performance of those systems which measure the elapsed phase or time between one zero-crossing of an oscillator signal and another such crossing or the original crossing delayed in time, such as coherent range and range-rate tracking systems or time-base measurement or generating systems, can be predicted in a first-order statistical sense by these deviation spectra. For example, the normalized rms range-error in a

coherent system caused by range-tone oscillator instability is described by

$$\frac{\sigma_R(\tau)}{\bar{R}(\tau)} = \frac{1}{2\pi \bar{f}} \left(\frac{1}{2\pi} \int_{-\infty}^{+\infty} S_\phi^{\cdot}(\omega) \cdot |H(\omega)|^2 \cdot \frac{\sin^2(\omega\tau/2)}{(\omega\tau/2)^2} \, d\omega \right)^{1/2} \qquad (7)$$

where τ is the two-way transmission time to and from target, $\sigma_R(\tau)$ is the rms range error, $\bar{R}(\tau)$ is the average or true range to target, and $|H(\omega)|^2$ is a linear-system characteristic function describing the phase-processing characteristic of the entire tracking system. This description of oscillator instability has distinct advantages over its predecessors in that the effect of a system characteristic function enters in a simple, explicit manner.

The determination of $S_\phi^{\cdot}(\omega)$ of a given oscillator permits the prediction of its performance in any number of different systems. Thus, any oscillator-stability measurement strategy must be evaluated in the light of its efficacy in yielding either $S_\phi^{\cdot}(\omega)$ or $S_\phi(\omega)$, regardless of what quantity is fundamentally measured, or how the measurement is conducted.

Most previous descriptions of oscillator zero-crossing stability have been based on the concept of a fractional frequency instability, defined as the rms deviation in frequency of an oscillation over a time τ divided by the average frequency during this interval. We have chosen to call this normalized quantity $I(\tau)$. Prior techniques for the measurement of oscillator instability have attempted to determine $I(\tau)$, usually through counting and accumulating time increments of an integral number of oscillation periods. The basic measured quantity is thus the period of an oscillation, whose rms value in a time τ divided by the accompanying average value can be shown to be approximately equal to $I(\tau)$, if the value of $I(\tau)$ for any given τ is small. Unfortunately, this technique does not readily yield the desired spectral information[3, 4], and we must choose an alternate technique.

Since there is a duality between correlation functions and spectral densities in any wide-sense stationary random process, we could obtain spectral data by a basic measurement of the autocorrelation function of the instantaneous frequency of an oscillation, or, for that matter, describe the performance of an oscillator in a system in terms of a correlation function. Such a description, however, would involve convolution integrals, and is not as tractable mathematically as Eq. (7) if both are formulated to yield those parameters of performance directly related to the left side of Eq. (7), particularly when a systems characteristic function (an impulse response) is involved. We prefer the spectral description. In a technique for the determination of spectra, correlation functions are an extra complication and a source of an extra empirical inaccuracy. Thus we propose to attack the problem of direct measurement of $S_{\dot{\phi}}(\omega)$ and/or $S_{\phi}(\omega)$.

1.3 Goals of Measurement System Performance

The requisite performance of the measurement system cannot be determined without some a priori knowledge of the constituents of the spectra we desire and some insight into the mechanisms involved in their creation. In addition, we must be cognizant of the theoretical limitations of spectral measurement and evolve some compensations or alternatives if these limitations prove important in our particular problem.

Equation (7) shows the necessity of an integration across the origin of the spectrum $S_{\dot{\phi}}(\omega) \cdot |H(\omega)|^2$. Since $H(j\omega)$ in any system within the class considered here is always some sort of lowpass characteristic, we may be certain that the low-frequency portion of $S_{\dot{\phi}}(\omega)$ is of major interest. There is always sufficient attenuation roll-off slope with increasing frequency in $|H(\omega)|^2$, such that the region $\lim_{\omega \to \infty} S_{\dot{\phi}}(\omega)$ will not be of interest, as we shall see. Figure 13, p. 53 of Ref. 1, shows the expected shape of $S_{\dot{\phi}}(\omega)$ of any oscillator, and the mechanisms underlying the various portions of the general

spectrum are described within the reference. The only constituent known to contribute a broad region of positive slope to $S_{\dot{\phi}}(\omega)$ is that caused by white noise added to the signal external to the basic oscillation mechanism. This external noise produces an ω^2 term in $S_{\dot{\phi}}(\omega)$. The logarithmic slope of this term is 6 dB/octave, such that arguments invoking the limiting action of $|H(\omega)|^2$ in Eq. (7) as $\omega \to \infty$ are upheld. In general, there also is adequate bandpass filtering in an oscillator after the oscillation loop to terminate the positive slope. There is a region of flat spectral density which is attributable to additive white noise within the oscillation loop. Finally, as $\omega \to 0$, there is a region of negatively sloped spectrum, whose asymptotic behavior is usually $a/|\omega|$. This is a theoretically predictable and an actually observed phenomenon generally considered to be the result of "flicker noise." The presence of the observed "random-walk" nature of the phase characteristic of an unlocked oscillator is predictable if $S_{\dot{\phi}}(\omega)$ has a nonzero density at the origin, so it is reasonable to presume that such is the case. Energy arguments are sufficient to insure that $S_{\dot{\phi}}(\omega)$ remains bounded throughout, so it is clear that an $a/|\omega|$ shape cannot prevail all the way to the origin. The precise behavior of $S_{\dot{\phi}}(\omega)$ at the origin is not known, and perhaps never will be; suffice to say that it levels or dips in some way as to be bounded, but not zero.

It is obvious that spectral information cannot be obtained either as $\omega \to \infty$ or $\omega \to 0$. The problem at $\omega \to 0$ is important considering the behavior of $S_{\dot{\phi}}(\omega)$, $|H(\omega)|^2$, and $\sin^2(\omega\tau/2)/(\omega\tau/2)^2$ as $\omega \to \infty$. Some alternative must be developed to handle the effect of $S_{\dot{\phi}}(\omega)$ close to the origin. In a real-time presentation, the slowly varying or long-term frequency effects of flicker noise are indistinguishable from those phenomena generally described as drift. If the instantaneous frequency of an oscillator signal is observed and sufficiently narrowband filtered, the drift phenomena approaches the appearance of a deterministic function of time, such as that shown in Fig. 1.

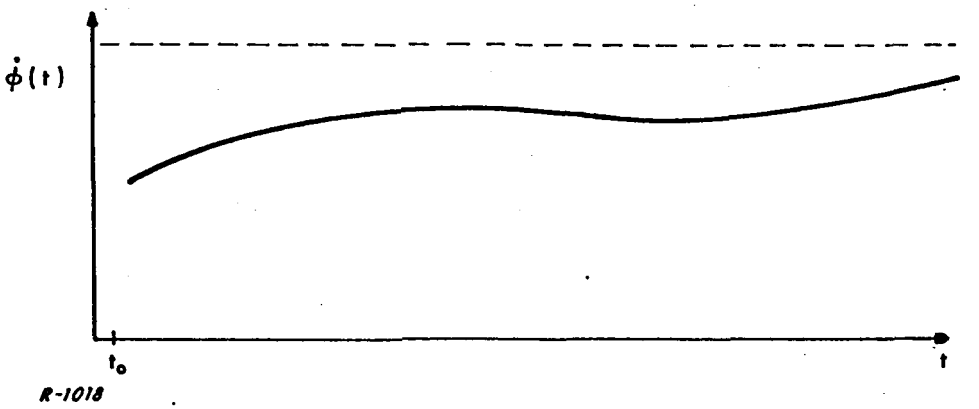

Fig. 1 Narrowband Filtered Frequency Process vs. Time.

With sufficient filtering (but not infinite averaging) we can approximate the random characteristic of the frequency by such a deterministic function of time. This approximation changes the characteristic of an initially distributed spectral region in $S_{\dot{\phi}}(\omega)$ to that of an impulse at the origin whose area is time-varying. Now, if we can determine the maximum bandwidth, called $2\pi B$, required to establish a reasonable approximation of this kind, we can lump that distributed spectrum from $\omega = 0$ to $\omega = \pm 2\pi B$ into a specular component at $\omega = 0$. The contribution to any system error of this component can be handled without recourse to random theory, and we can handle the problem at $\omega \to 0$ by eliminating the region $-2\pi B \leq \omega \leq 2\pi B$ from the kernel of Eq. (7). Nevertheless, $1/2\pi B$ may represent such a long time that spectral measurement in this region may still be impractical. It is reasonable to presume, however, that $S_{\dot{\phi}}(\omega)$ will retain its shape all the way to $|\omega| = 2\pi B$ once the $a/|\omega|$ flicker component becomes dominant as $|\omega|$ decreases toward zero. Thus, it seems necessary only to preserve spectral resolution toward the origin until the flicker-noise spectrum is determined with sufficient accuracy, and then extend the shape toward the origin as far as it is necessary for the purposes of analysis. It appears that conventional period counting techniques are adequate to measure the quasi-deterministic drift curve.

The relative strength of constituents in a given $S_\phi^{\cdot}(\omega)$ reflects the type of oscillation. For example, a hard oscillation such as that produced by a VCO oscillator running unlocked would have a small additive noise ω^2 spectral component and relatively large flat-spectrum and $a/|\omega|$ components. A weak oscillation designed for maximum long-term stability, such as that from atomic frequency standards, would have a large ω^2 component, and small flat and $a/|\omega|$ components. Since it is the small $|\omega|$ region of $S_\phi^{\cdot}(\omega)$ that represents the "long-term" properties of frequency instability, it is reasonable to presume that atomic standards, being the most long-term stable of any class of oscillators, would exhibit minimum flicker components. The authors have seen proof that $1/2\pi B$ of one hour represents adequate average time for the quasi-deterministic drift approximation to hold in the case of a hydrogen maser whose long-term stability seems to be the best yet observed. By this reasoning, a lower limit of $\omega = 1/1$ hour, or $\omega = 1/2$ hour, is probably adequate for spectral resolution in general.

It has been shown[5] that the optimum stability and accuracy in convergence to the spectral density of a real-time process is assured if the corresponding spectral density is flat, i. e., a constant. In light of the anticipated $S_\phi^{\cdot}(\omega)$ components it is clear that we should measure $S_\phi^{\cdot}(\omega)$ for all $|\omega| \leq \omega_o$, where ω_o is that value where external additive noise dominates $S_\phi^{\cdot}(\omega)$ as $|\omega|$ increases, and we should measure $S_\phi(\omega)$ for $|\omega| \geq \omega_o$. This choice affords the flattest spectrum available in any range of ω without any additional "prewhitening" filtering.

The accuracy requirements for the measurement are not extreme, at least initially. The technique is new, and almost any spectral data that can be obtained will be superior to previous information for this class of applications. The immediate goals are sensitivity and freedom from drift. It is clear that the

threshold of the test set, defined as those minimum residual spectral densities calibrated in units of $S_{\dot{\phi}}(\omega)$ and $S_{\phi}(\omega)$ that are present at the output of the device and are caused by the measurement device itself, independent of the input oscillator source or sources, will have to be extremely low. Exactly how low these residual spectra must be cannot be known before oscillator measurements are made and the state of the oscillator art in terms of $S_{\dot{\phi}}(\omega)$ is determined. The sensitivity of the test set is thus a post facto requirement. The same can be said of drift, although we have a reasonable limit on the maximum time interval over which drift must be considered. It is also clear that careful control of time constants and bandwidths must be maintained to eliminate any significant coloration of the measured oscillator instability spectra and to prevent any AM to PM conversion effects. The sensitivity requirement is made more formidable by the necessity of the tremendous rejection of the $2\pi \bar{f}$ portion of $\dot{\theta}(t)$, as seen in Eq. (3), that must be accomplished before instability can even be detected. As might be expected, these requirements have led to difficult design problems and some sophisticated techniques for their solution. These are described in detail in the following sections.

2. SYSTEM DESCRIPTION AND OPERATION

2.1 Principle of Operation

The basic configuration of the measurement system was described in Sec. 4.4 of Ref. 1. It consists of three functional sections as shown in Fig. 2: the signal extraction and processing section, the error multiplication section, and the output analysis section.

It was shown in Sec. 4.3 of Ref. 1 that the requisite rejection of the average-frequency (f) cannot be achieved with one oscillator signal alone. Thus, two independent oscillators, generating two 1 MHz oscillations at almost identical average frequencies, supply inputs to the measurement system. An automatic detection loop, incorporated in the signal extraction and processing section, maintains a synchronous quadrature relationship between these two signals, thus essentially removing all average frequency drifts.

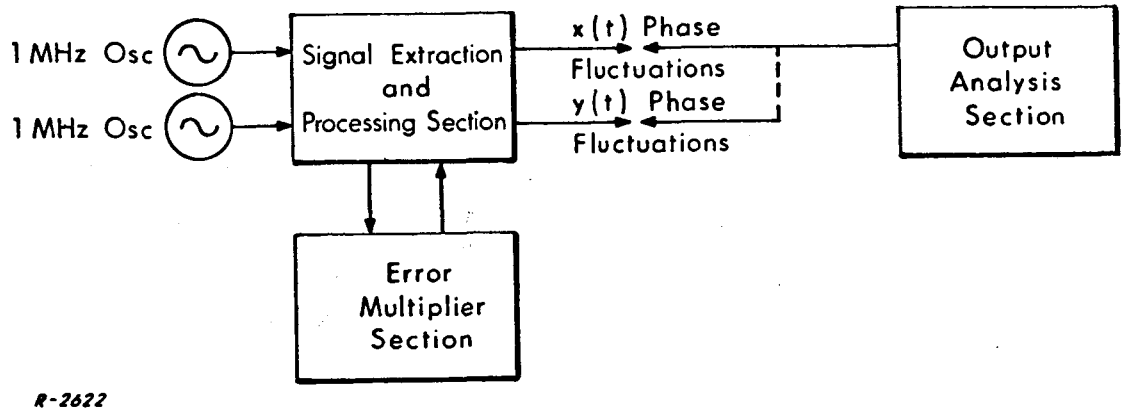

Fig. 2 Basic Configuration of the Measurement System.

The automatic-detection loop, illustrated in simplified form by Fig. 3, is essentially a second-order electromechanical phase-locked loop. The motor and RF resolver operate on one of the two input oscillations to simulate a VCO. The average frequency difference between the two oscillators, denoted by $\Delta\bar{f}$ and representing the relative phase drift between the two oscillators, can be seen to be analogous to a doppler offset frequency in a conventional tracking PLL.

The particular implementation of the automatic-detection loop shown in Fig. 3 has certain desirable properties. The loop has been designed so that the locked-loop transference from input frequency difference to the lowpass output y(t) is maximally flat (second-order Butterworth). Thus, this output is analogous to an FM discriminator output for all difference-frequency fluctuation components occupying the spectrum from dc almost up to ω_c, the loop cutoff frequency. However, it has certain advantages over an FM discriminator output. First, there is no long term or temperature-dependent center-frequency drift. Second, because of the loop lowpass characteristic, the high-frequency fluctuation components are greatly attenuated (at 12 dB per octave). Third, the basic sensitivity before dc gain of 2π volts per hertz is very high.

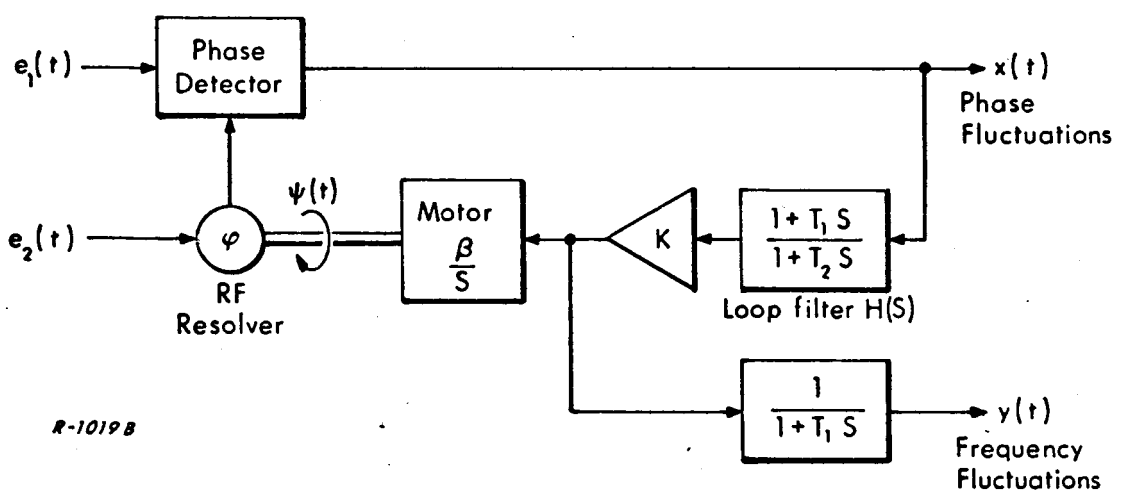

Fig. 3 Basic Configuration of the Automatic-Detection Loop.

The locked-loop transference from input phase difference to the high-pass output x(t) is flat from frequencies slightly greater than ω_c. Thus, this output is analogous to a phase detector output, but it too has certain advantages over conventional open-loop techniques. Since the signals are continuously maintained in quadrature at the detector, several problems are eliminated. First, there is no variation in the phase-to-voltage transference with changing phase. Second, the rejection of AM components is maximized, and this too, does not vary with changing phase. Third, there is no abrupt change in the output signal at 2π intervals as happens in open-loop systems. In addition to these advantages, the system possesses a high phase-to-voltage sensitivity of 10 volts per radian before post-amplification which, combined with a low noise level, provides very high signal-to-noise ratio.

The automatic-detection loop thus provides two output signals: the first, x(t), is a signal proportional to the phase-difference fluctuations passed through a maximally-flat highpass filter; while the second, y(t), is a signal proportional to the frequency-difference fluctuations passed through a maximally-flat lowpass filter. These two output signals are fed, after amplification and interfacing, to the output analysis section.

The output analysis section contains primarily a low-frequency spectral-density analyzer, which can process either x(t) or y(t) and graphically display the corresponding spectrum. Spectral analysis at frequencies below the lower frequency limit of the analyzer can be accomplished by recording and digital processing of the fluctuations. Providing that the statistical independence of all oscillator fluctuations is assured, two-at-a-time measurements upon three oscillators are sufficient to determine the fluctuation spectra of each.

The predetection error multiplier section is a group of frequency multipliers and mixers operating on the two 1 MHz oscillator signals whose phase or frequency fluctuation spectra are to be measured. Error multiplication provides effective predetection gain on the phase and frequency fluctuations, and hence an increase of the overall sensitivity of the measurement system, where

sensitivity is defined as the lowest spectral densities $S_{\phi}(\omega)$ or $S_{\dot{\phi}}(\omega)$ that can be reliably measured. To couple properly with the automatic detection loop, the error multiplier accepts 1 MHz signals as inputs and provides 1 MHz signals as outputs with enhanced phase and frequency fluctuations.

2.2 Physical Description

The three sections of the measurement system were fabricated in the form of several self-contained chassis. The sections were chosen for pedagogical purposes; here we are concerned with the optimum grouping of circuits into chassis in terms of signal isolation, maintenance, and the feasibility of future improvement of the test set. Thus we have designed and constructed according to a minimum signal processing approach, and have organized the test set as an interconnection scheme between rack-mounted self-contained chassis. Each of these chassis presents standard 50 ohm input and output impedances (with the exception of the output analysis section), permitting rapid changing of chassis. As improvements in circuitry are made, the measurement system can be updated within minimum difficulty. Inherent in the operation of the system is the need to change various gains, loop time constants, and operating modes. We have attempted to make this operation as simple as possible with the aid of switches and control knobs. Figure 4 is a pictorial representation of the equipment. The physical and electrical features of the equipment are described in detail in the next few sections.

2.3 Description of the Signal Extraction and Processing Section

The signal extraction and processing section consists of three chassis and a reference source, interconnected as shown in Fig. 5. The three chassis are the baseband chassis, the electromechanical chassis and the RF chassis. The reference source is a General Radio 1115-B standard frequency oscillator.

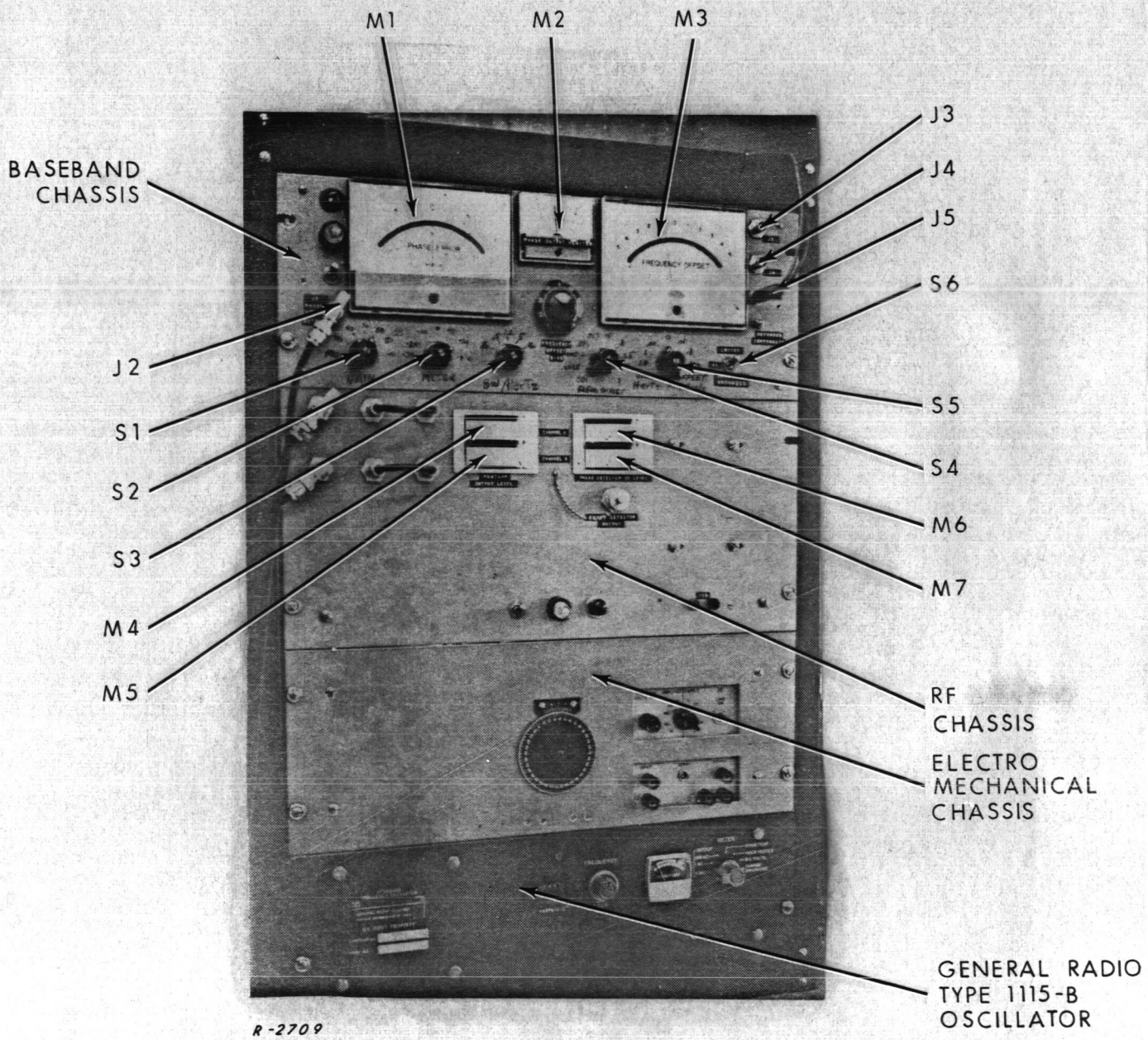

Fig. 4(a) Prototype Equipment, the Signal Processing and Extraction Section.

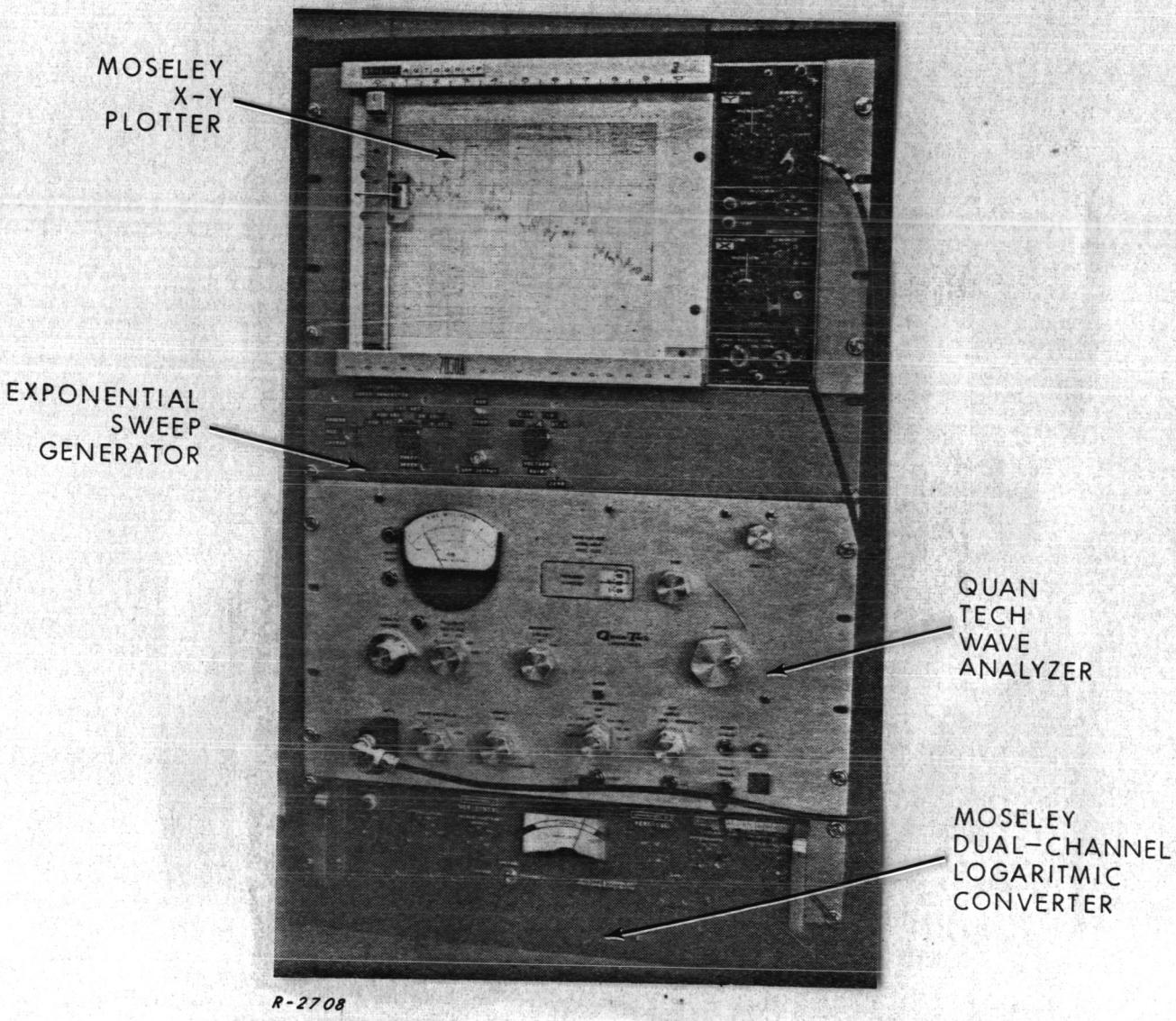

Fig. 4(b) Prototype Equipment, the Output Analysis Section.

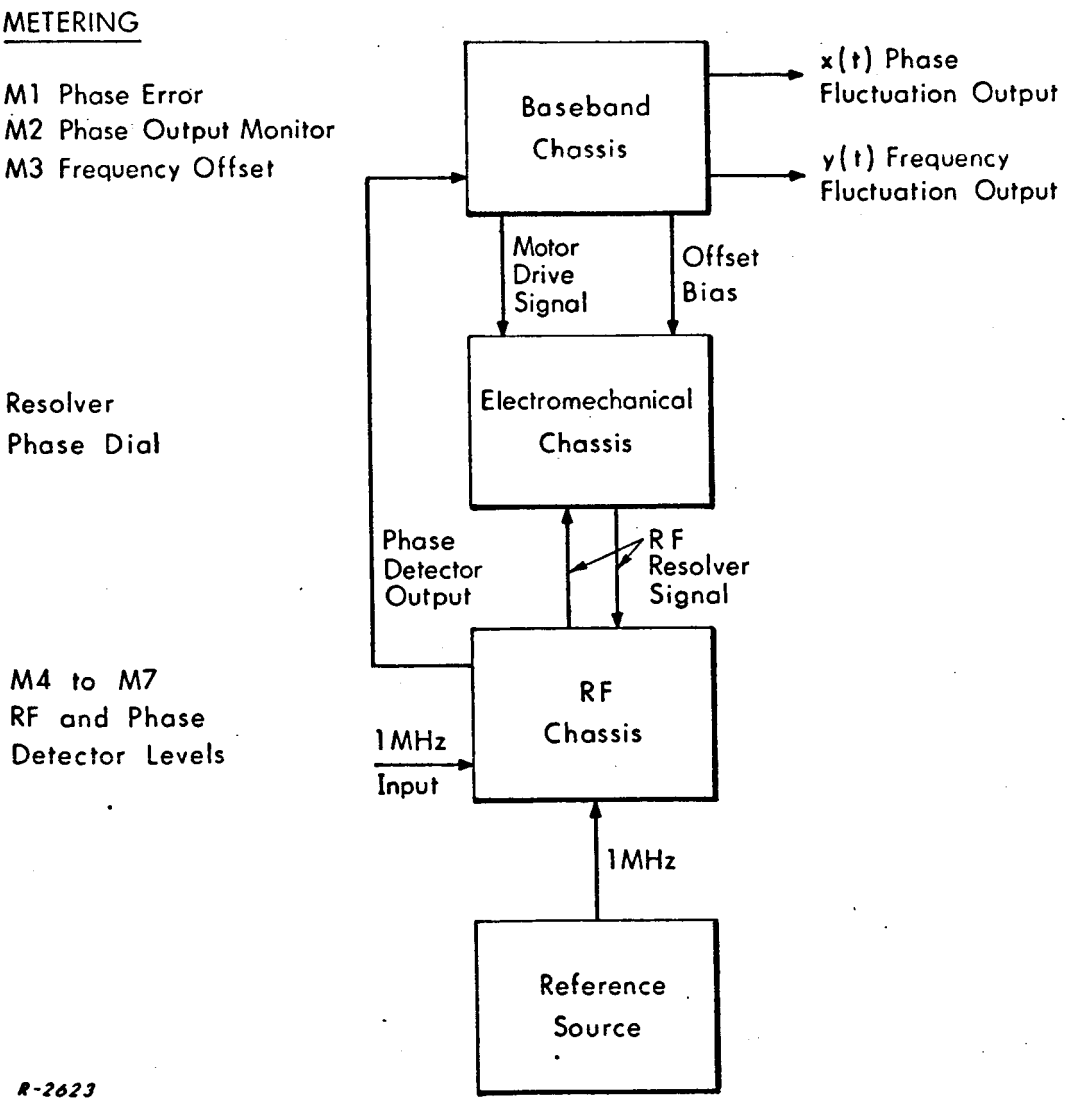

Fig. 5 Signal Extraction and Processing Section.

The RF chassis, in conjunction with the resolver in the electromechanical chassis, processes the two 1 MHz input signals and produces an output consisting of the instantaneous phase difference between the two signals including all phase components from dc to about 10 kHz.

The baseband chassis accepts the phase-difference signal and operates on it to provide an error voltage for the motor which drives the resolver, thus closing the phase-locked loop. In addition, it provides selectable gain and meter indicators for both the highpassed phase difference signal x(t) and for the lowpassed frequency-difference signal y(t).

The electromechanical chassis contains the RF resolver, its drive motor, and dc amplifier. The motor is a dc servo type with a speed-to-voltage transference of about 5 rad per sec/volt. A tachometer/generator is integrally mounted with the motor and is used in a feedback loop around the motor to reduce the minimum stiction speed and to adjust the total speed-to-voltage transference (β) of the servo loop to 1.0 radians per sec/volt.

A General Radio Type 1115-B Standard Frequency Oscillator supplies a 1 MHz signal for reference. However, if other signals of reference quality are available, they can be substituted.

The chassis are described in more detail below.

The RF chassis accepts the two 1 MHz input signals in channels A and B, as shown in Fig. 6. Channel A drives the split-phase input of the phase detector. Channel B, after passing through the resolver, drives the series input of the phase detector.

The signal conditioners at the input of each channel produce +20 dBm output for any input signal amplitude between -13 dBm and +17 dBm. The output of the signal conditioner in each channel is brought to the front panel and patched into the following amplifier on a coaxial cable. This allows the error multiplier to be inserted in either channel at this point. After the error multiplier patch,

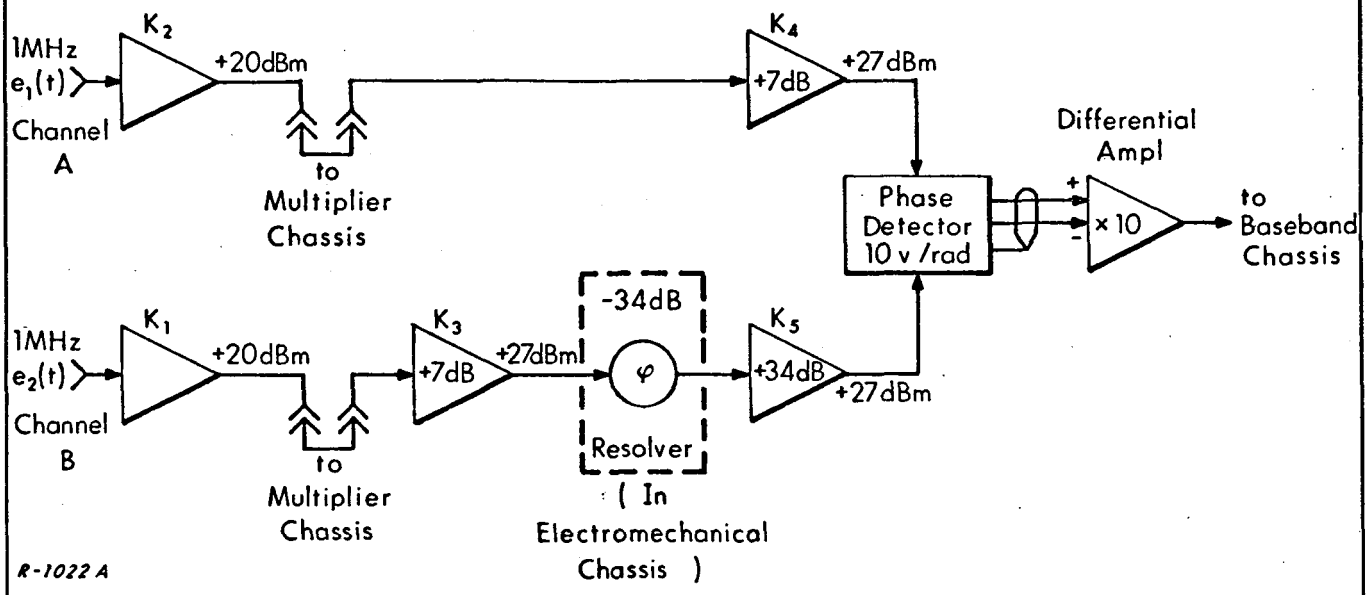

Fig. 6 Block Diagram of the RF Chassis.

each channel has a 7 dB power amplifier. Channel A goes directly to the phase detector while channel B is passed through the resolver and a 34 dB post-amplifier, which makes up for the attenuation of the resolver, and is then fed to the phase detector. The RF levels at the input to the phase detector must produce readings of 85 ± 2 on M4 and M5 to maintain the phase detector transference for proper system operation. The resolver is driven by the servo motor in such a way that the two signals are maintained in quadrature at the phase detector.

The phase detector is fed by two equal-amplitude sinusoidal signals. This ensures maximum sensitivity to PM fluctuations and minimum sensitivity to AM fluctuations. The phase detector is set up for a transference of 10 volts/radian. The dc level of the phase detector output is indicated on M6 and M7, and is available on the front panel of the RF chassis in a Twinax connector. M6 and M7 must read 76 ± 2 for proper system operation. When the phase-lock loop is out of lock, M6 and M7 will oscillate in quadrature. The differential amplifier subtracts the two outputs of the phase detector and produces a single-ended output at 100 volts/radian clipped at ±12 volts. The net characteristic of

the RF section is a high gain phase-to-voltage transference which is independent of the RF input level and which possesses a high dynamic range of phase linearity.

The baseband chassis contains the loop filter for the phase-locked loop, the output amplifiers for x(t) and y(t) phase and frequency fluctuation outputs, and the offset bias controls, as well as metering of the system operation as shown in Fig. 7.

The input signal from the output of the phase detector differential amplifier is applied to the rear connector J1. Since this signal consists of the phase fluctuations, it is amplified with gain from 0 to 60 dB selectable in 10 dB steps by S1, and brought out to the front panel connector J2 as the x(t) output at levels of -40 to -100 dB with respect to a radian (dB rad) per volt of output. There are two meters connected to this output line. M1, labeled "phase error," is a center-zero dc meter with voltage sensitivity selected by switch S2 from 30 millivolts (-30 dB) full scale to 30 volts (+30 dB) full scale in 10 dB steps. This switch should never be left on a range lower than 10 volts (+20 dB) as the amplifier can severely overload the meter. The high sensitivity ranges are only for setup and calibration and are not normally required in the operation of the system. This meter indicates the dc and very low frequency (less than 2 Hz) components of the x(t) output. M2, labeled "phase output monitor," is a 10 volt full scale peak reading voltmeter. This meter monitors the total (dc plus ac) peak level of the x(t) output and is used to indicate the maximum safe gain for that output. For linear operation the peak phase level should never be allowed to exceed 50% on this meter. If the output level exceeds 100% then the output amplifier will be severely clipping the signal, thus resulting in a degraded or erroneous output spectrum. To correct this condition the gain setting of S1 should be reduced such that M2 reads less than 50%. The system has been so designed that it does not saturate as long as M2 reads less than 50% for some setting of S1.

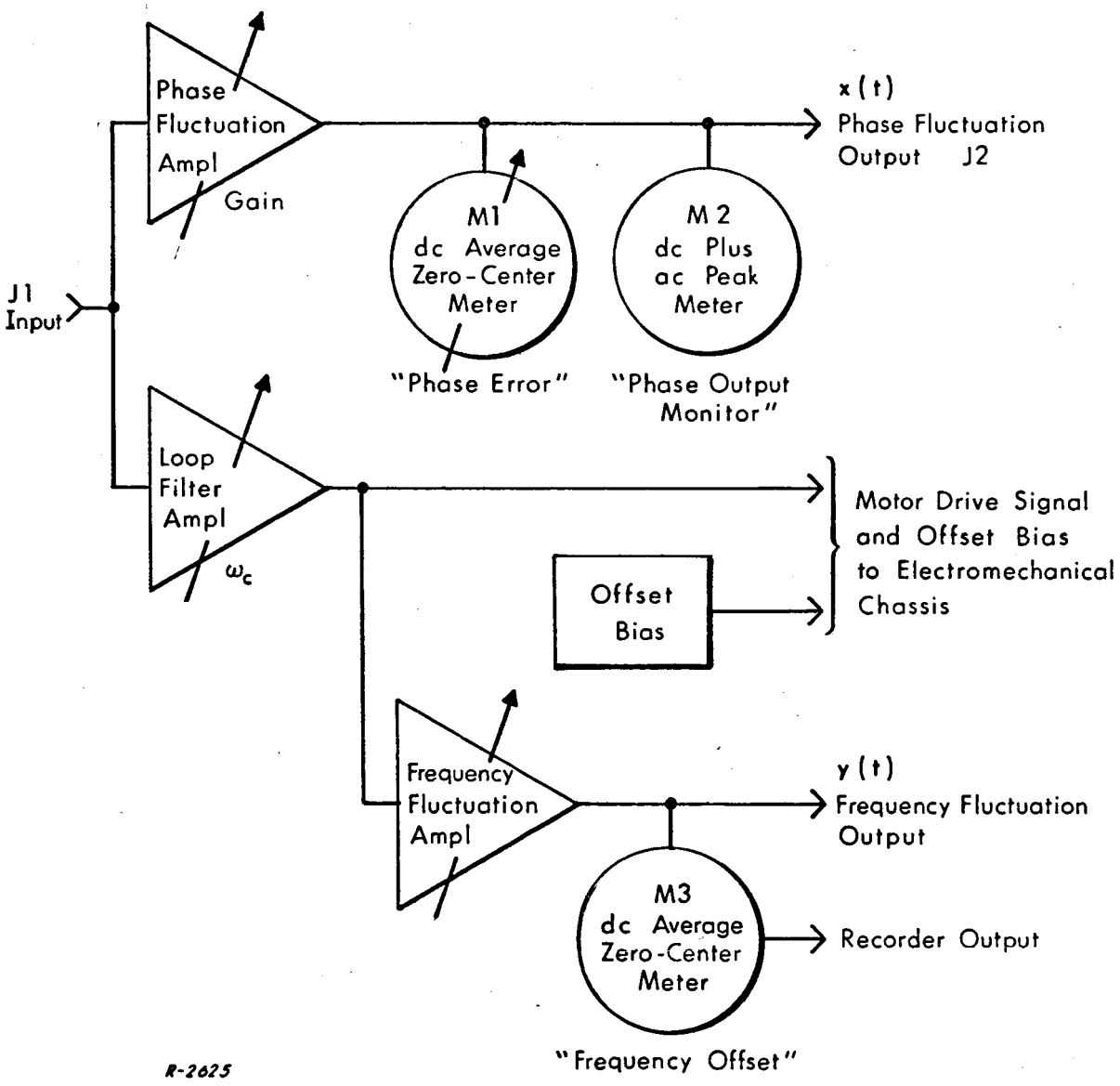

Fig. 7 Block Diagram of the Baseband Chassis.

The input signal from the RF chassis is also applied to the loop filter/amplifier. The feedback time constants of this amplifier are selected by S3 so that the loop cutoff frequency ω_c is adjusted in 5 dB steps of 0.16, 0.5, 1.6, 5, and 16 Hz. In the 5 and 16 Hz settings the loop will generally acquire a new signal or eliminate a forced transient in a very few seconds. The normal acquisition procedure is to select the widest loop bandwidth, and then trim the bias until the phase error meter M1 indicates synchronous operation. M1 responds to the finitely averaged phase detector output, and will null when the loop is in proper trim. Once the loop acquires, ω_c can be switched to a lower value with only a short pause to allow minor perturbations to die out and data can then be taken.

The output of the loop filter/amplifier goes to the y(t) output amplifier and to the electromechanical chassis. In the 16 Hz range of ω_c a large transient can cause the loop to oscillate. This oscillation appears on the resolver dial and the meters, and can be stopped by temporarily damping the dial by hand.

The y(t) output is derived from the signal at the input to the electromechanical chassis and is compensated by an amplifier whose upper frequency roll-off is the same as ω_c and is also selected by S3. The signal at the input to the y(t) output amplifier is 2π volts per Hertz of frequency offset. The y(t) output amplitude is controlled by S4 and appears on the display panel at two BNC connectors labeled J3 and J4 for ±10 volt full scale measurement; one phone jack, J5, for current measurement of ±0.5 MA into 1400 ohms; and on the "Frequency Offset" meter, M3, which is calibrated in Hertz. Full scale range are ±0.001 to ±1.0 Hertz in 1, 2.5, 5 sequences for convenient linear recording on a ± 5 division strip chart.

When two oscillator signals which have a nonzero average frequency offset are to be analyzed, a calibrated dc bias can be introduced at the input of the electromechanical chassis to allow increased sensitivity of the y(t) output and to reduce the possibility of saturation in the loop amplifiers. The magnitude of the error signal and the deflection of the frequency offset meter will be reduced

by the amount of bias added. This bias can be adjusted to produce a zero-average reading on the frequency offset meter for a constant frequency offset. Switch S5 and the ten-turn potentiometer control labeled "offset bias" determine the amount of bias injected into the system, and are calibrated in Hertz with full-scale ranges of -1.0, -0.1, -0.01, 0, +0.01, +0.1, +1.0 Hz and a vernier of 0-1000 for the range selected. Thus there is a frequency resolution of 10^{-5} Hz in the bias setting.

The electromechanical chassis, illustrated in Fig. 8, consists of the RF resolver, motor/tachometer, feedback amplifiers and power amplifier. The tachometer and amplifiers are used in a feedback loop, called the minor loop, around the motor. This loop serves to reduce the effective sticktion of the motor by three orders of magnitude to an acceptable level. The shaft of the resolver is coupled to a front-panel indicator dial which is graduated in degrees. This dial rotates with the motor of the resolver and directly indicates the phase shift introduced on the signal in channel B. The input and output terminals of the power amplifier are available on the front panel.

2.4 Description of the Output Analysis Section

There are two output signals from the baseband section; one is directly proportional to the highpassed phase fluctuations x(t), and the other is directly proportional to the lowpassed frequency fluctuations y(t). The output analysis section, illustrated in Fig. 9, provides direct analog spectral analysis of either of these signals in the frequency range of 1 to 5000 Hz. The two outputs of the analysis equipment are a signal proportional to the spectral density at a particular frequency and a signal proportional to that frequency. The heart of the analysis equipment is a Quan-Tech Laboratories modified model 304-R Wave Analyzer (Spec. 2222). This analyzer provides both manual and automatic frequency sweep, selectable bandwidths and averaging times, selectable sweep spans and rates, and linear dc analogs as output functions. A Moseley 7560A dual-channel logarithmic converter is used to provide linear decibel and logarithmic frequency versions of the wave analyzer outputs. Thus, with this

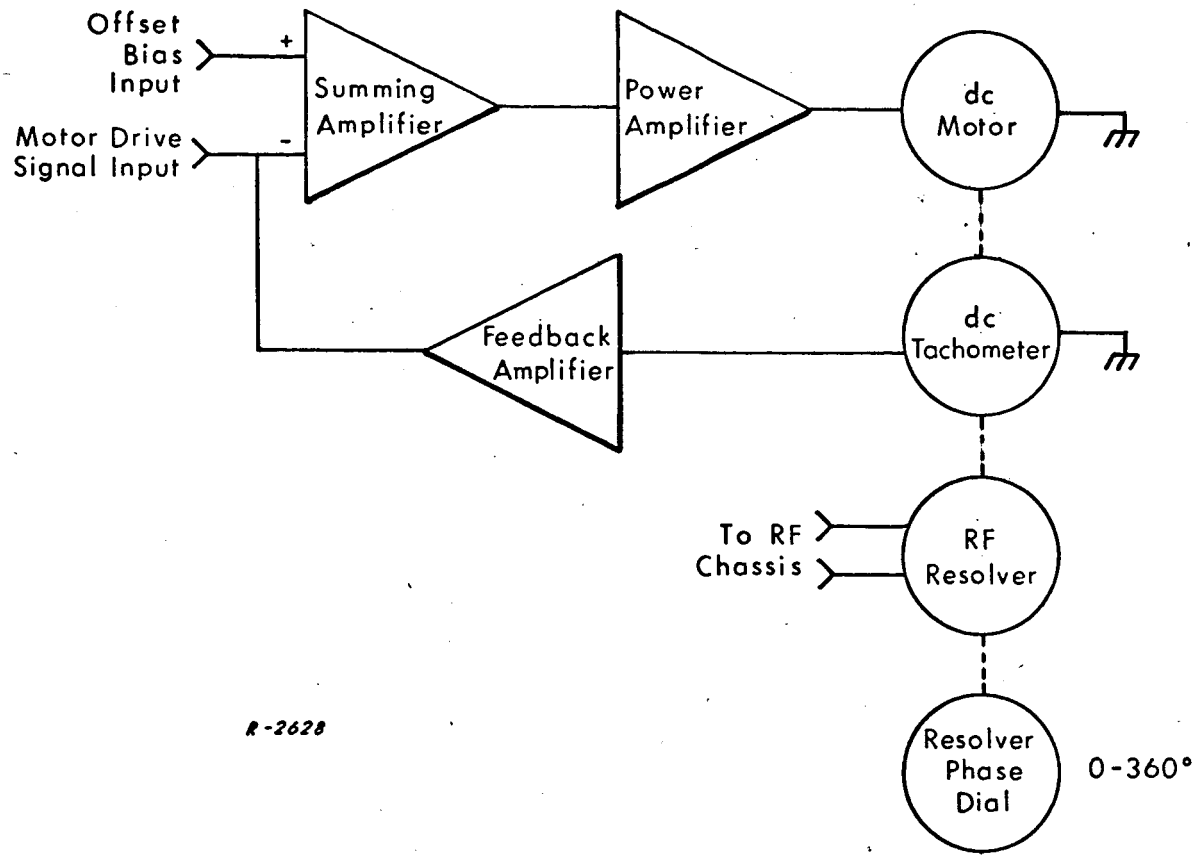

Fig. 8 Block Diagram of the Electromechanical Chassis.

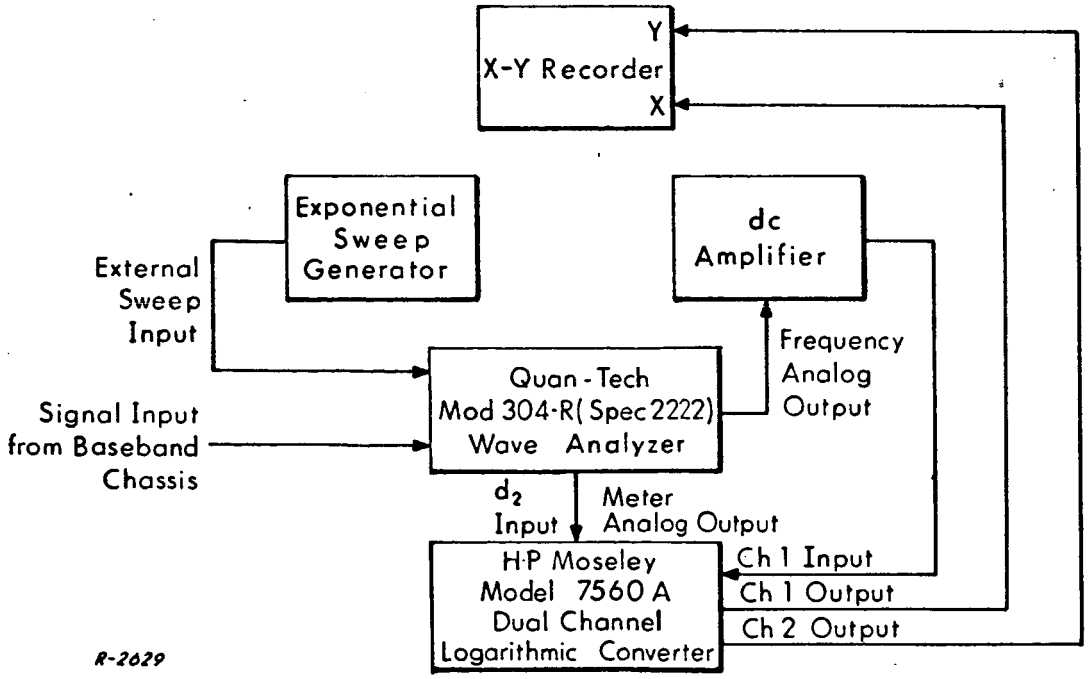

Fig. 9 Block Diagram of the Output Analysis Section.

combination, the output presentation on the X-Y recorder can have either linear or logarithmic amplitude and frequency scales to best fit the signals being processed. The amplitude scale (y-axis) is usually operated in the logarithmic mode and has about 50 dB dynamic range. The frequency scale (x-axis) is operated linearly for presentation of line frequency and other harmonically related components, and is operated logarithmically for broadband components to facilitate interpretation of signals which vary exponentially with frequency (such as 1/f). The exponential sweep generator may be used for logarithmic frequency measurements to provide a constant sweep speed of the pen along the x-axis, and thus a constant effect from the averaging time constant in the amplitude output. The Quan-Tech wave analyzer produces a dc frequency analog output of 1 millivolt per Hertz (i.e., 0–5 volts for 0–5 kHz). The minimum useful input to the logarithmic converter is about 10 millivolts, thus a dc amplifier is used to compatibly interface these units when low frequencies are used.

2.5 Description of the Error Multiplier Section

The error multiplier section, shown in Fig. 10, is a self-contained unit which can be patched into either channel to multiply the spectral distribution and offset of the oscillator instabilities in that channel by a factor of 16. The error multiplier requires a 5 MHz input at +14 dBm as input to J6. The 1 MHz signal to be multiplied must be applied to J7 at +20 dBm level, either separately generated or as the output of a signal conditioner. The 1 MHz signal is multiplied in four doublers to 16 MHz and the 5 MHz signal is tripled to 15 MHz. These two signals are mixed and the resultant 1 MHz signal is filtered and amplified to +20 dBm at J8. The Type 1115-B Standard Frequency Oscillator supplied with the system provides 5 MHz at +14 dB and has a 1 MHz output which can be used as the reference signal.

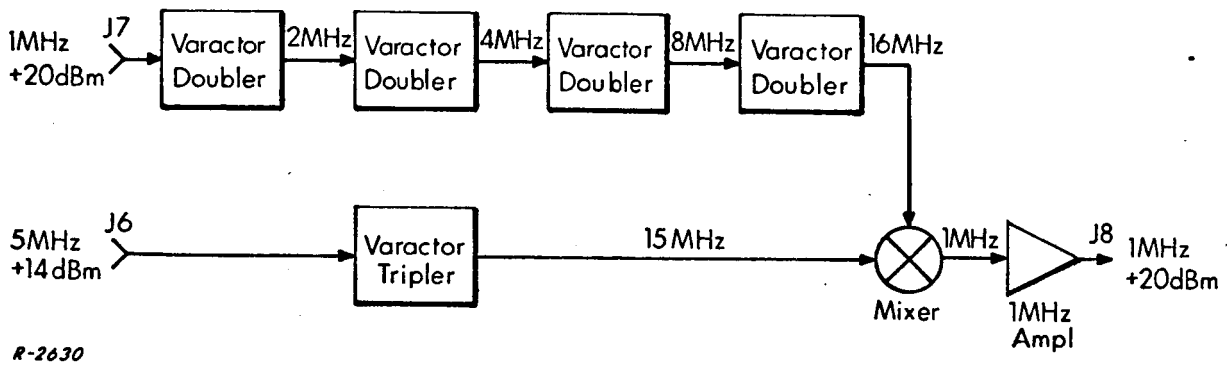

Fig. 10 Error Multiplier Section.

3. ANALYSIS AND DESIGN OF THE AUTOMATIC-DETECTION LOOP

3.1 Analysis of the Ideal Loop

A linearized model of the automatic-detection loop, shown in Fig. 11, represents the behavior of the loop under lock conditions. Let the two input signals to the loop be described by

$$e_1(t) = a_1(t) \cos \theta_1(t) \tag{8}$$

and

$$e_2(t) = a_2(t) \cos \theta_2(t) \tag{9}$$

where $\theta_1(t)$ and $\theta_2(t)$ have the same components as described in Eq. (2). K_1 is the total loop gain exclusive of the motor, and thus includes the transference of the phase detector – which in turn depends on the amplitude of the input signal – as well as those gains associated with amplifiers within the loop. β is the shaft-rotation-rate to input-voltage of the idealized minor loop expressed in radians per sec/volt, and $\psi(t)$ is the resolver shaft position or radians of phase shift introduced by the resolver in a non-modulo 2π or open-ended sense.

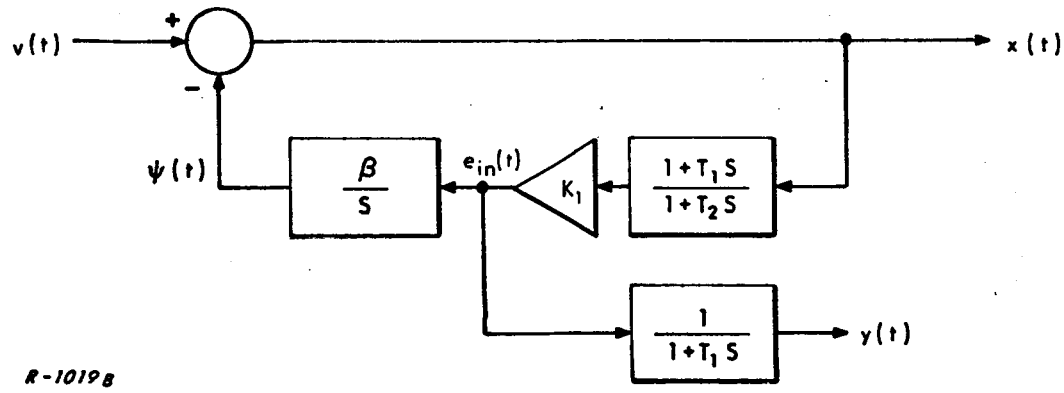

Fig. 11 Linearized Model of the Automatic Detection Loop.

As explained in Ref. 1 the input v(t) to the linearized model is the instantaneous phase difference, written as

$$v(t) = A\,[2\pi\Delta\bar{f}\,t + \Delta\phi(t)] \tag{10}$$

where we have defined

$$\Delta\bar{f} \triangleq \bar{f}_1 - \bar{f}_2 \tag{11}$$

and

$$\Delta\phi(t) \triangleq \phi_1(t) - \phi_2(t) \tag{12}$$

of Eq. (8) and Eq. (9). Under conditions of lock, the resolver rotates at a rate equal to $2\pi\Delta\bar{f}$ in order to preserve the synchronous, quadrature relationship at the detector input. By a proper selection of parameters, we can establish that the linear transfer functions of the loop are

$$\frac{X(s)}{V(s)} = \frac{s(s+1/T_2)}{s^2 + \sqrt{2}\,\omega_c s + \omega_c^2} \tag{13}$$

and

$$\frac{Y(s)}{V(s)} = \frac{s(1/\beta)\,\omega_c^2}{s^2 + \sqrt{2}\,\omega_c s + \omega_c^2} \tag{14}$$

where the parameter choices satisfy the conditions

$$\frac{K_1\beta}{T_2} = \omega_c^2 \quad , \tag{15}$$

$$\frac{K_1\beta\,T_2 + 1}{T_2} = \sqrt{2}\,\omega_c \quad , \tag{16}$$

and

$$K_1\beta T_1 \gg 1. \tag{17}$$

Utilizing Eqs.(10),(13) and (14) and accounting for the dc components generated by the phase detector to maintain lock, we show in Appendix A that the output spectral densities are given by

$$S_x(\omega) = A_1 \left\{ \frac{\omega^2(\omega^2 + 1/T_2)^2}{\omega^4 + \omega_c^4} \left[S_{\phi_1}(\omega) + S_{\phi_2}(\omega) \right] + \left(\frac{2\pi\Delta\bar{f}}{K_1\beta} \right)^2 \delta(0) \right\} \tag{18}$$

and

$$S_y(\omega) = A_2 \left\{ \frac{(1/\beta)^2 \omega_c^4}{\omega^4 + \omega_c^4} \left[S_{\phi_1}(\omega) + S_{\phi_2}(\omega) \right] + \left(\frac{2\pi\Delta\bar{f}}{\beta} \right)^2 \delta(0) \right\} \tag{19}$$

where A_1 and A_2 are calibration factors. Inequalities (16) and (17) establish that $1/T_2$ is small enough to be negligible within the passband of the filtering characteristic in Eq. (18), so that we have

$$S_x(\omega) \approx A_1 \left\{ \frac{\omega^4}{\omega^4 + \omega_c^4} \left[S_{\phi_1}(\omega) + S_{\phi_2}(\omega) \right] + \left(\frac{2\pi\Delta\bar{f}}{K_1\beta} \right)^2 \delta(0) \right\} \tag{20}$$

Both Eq. (18) and Eq. (20) show highpass filtering functions operating on the sum of $S_{\phi_1}(\omega)$ and $S_{\phi_2}(\omega)$. This sum is the spectrum of the difference-phase fluctuations $\Delta\phi(t)$, which we denote by $S_{\Delta\phi}(\omega)$. Equations (19) and (20) show complementary second-order Butterworth (maximally-flat) lowpass and highpass filtering operating on $S_{\Delta\phi}(\omega)$ and $S_{\Delta\phi}(\omega)$ respectively. Thus, they both have the same 3 dB cutoff frequencies, ω_c. Chapter 1 has established that these are precisely the filtering functions desired for the measurement of the constituents of the oscillator instability spectra.

We shall show in the next two sections that the practical limitations in the minor-loop design make it impossible to exactly achieve these maximally-flat characteristics. We shall then show how the actual design approximates these characteristics.

3.2 Analysis and Design of the Minor Loop

The block diagram of the electromechanical chassis shown in Fig. 8 may be simplified into the one shown in Fig. 12. In turn, a linearized model of the minor loop can be drawn as in Fig. 13. If we may neglect all time constants in the amplifiers, we may write the closed loop transference from $e_{in}(t)$ to $e_o(t)$ as

$$\frac{E_o(s)}{E_{in}(s)} = \frac{K_3K_4M(s)T(s)}{1 + K_3K_4M(s)T(s)} \tag{21}$$

where T(s) is the transference of the tachometer, and M(s) is the transference of the motor.

We choose to lump all mechanical effects of the motor, tachometer, and resolver into the mechanical time constant of the motor. To a first approximation,

$$M(s) = \frac{K_2}{s(1+T_e s)(1+T_m s)} \tag{22}$$

where T_e is the electrical time constant of the motor armature, and T_m is the mechanical time constant of the armature and shaft loading. If the loading impedance on the tachometer is high enough, we may neglect any electrical time constant in the tachometer, so that its transference becomes pure differentiation:

$$T(s) = \alpha s \tag{23}$$

Inserting (22) and (23) in (21) we obtain

$$\frac{E_o(s)}{E_{in}(s)} = \frac{\alpha K_2K_3K_4}{\alpha K_2K_3K_4 + (1+T_e s)(1+T_m s)} \tag{24}$$

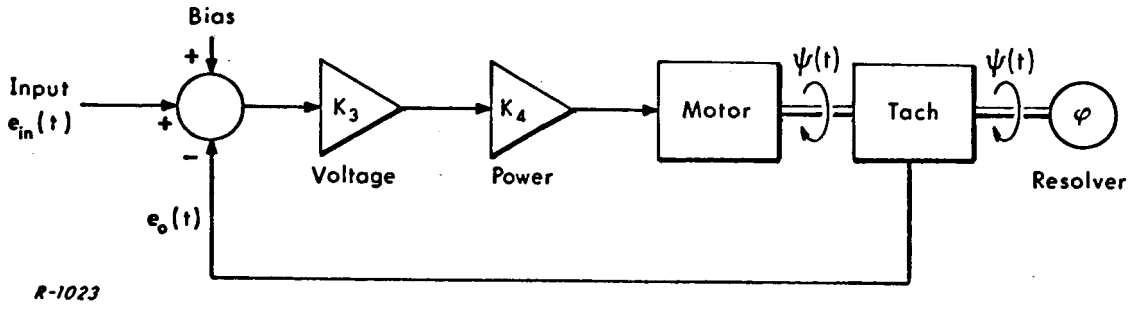

Fig. 12 Block Diagram of the Minor Loop.

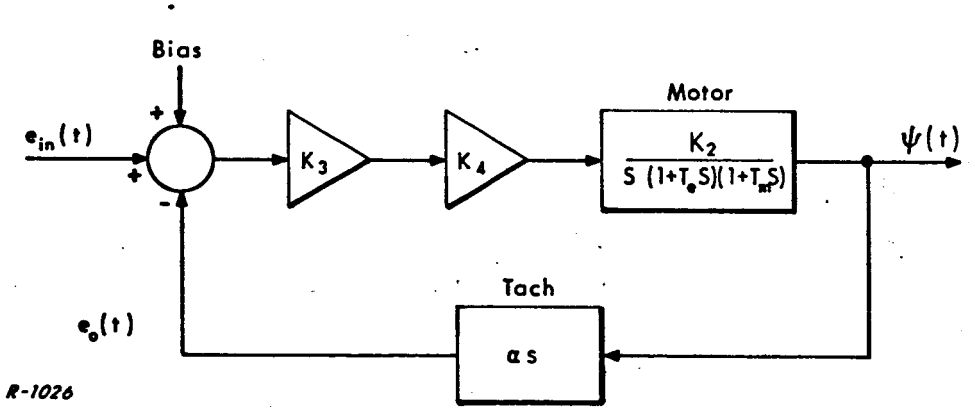

Fig. 13 Linearized Model of the Minor Loop.

The effective bandwidth of the transference $e_{in}(t)$ to $\psi(t)$ is required to be sufficiently wide to introduce negligible distortion of the automatic-detection loop filtering functions shown in Figs. (13) and (14). The largest ω_c we select will produce the most susceptibility to minor-loop bandwidth. It is clear that the effect of this bandwidth will be observable first at the $\Delta\phi(t)$ output of the automatic-detection loop, in that this output contains the highest frequency components. In general, the transference M(s) will not be sufficiently wideband, so that the feedback in the minor loop will be required to widen this bandwidth.

Let us plot a sample root-locus of the open loop (to unity feedback point) transference:

$$K_3K_4M(s)\,T(s) = \frac{\alpha K_2K_3K_4}{T_eT_m}\,\frac{1}{\left(s+\frac{1}{T_e}\right)\left(s+\frac{1}{T_m}\right)} \qquad (25)$$

This plot is shown in Fig. 14. T_m is sufficiently large so that the pole located at $\sigma = -1/T_m$ lies very close to the origin. As the loop gain is increased, the

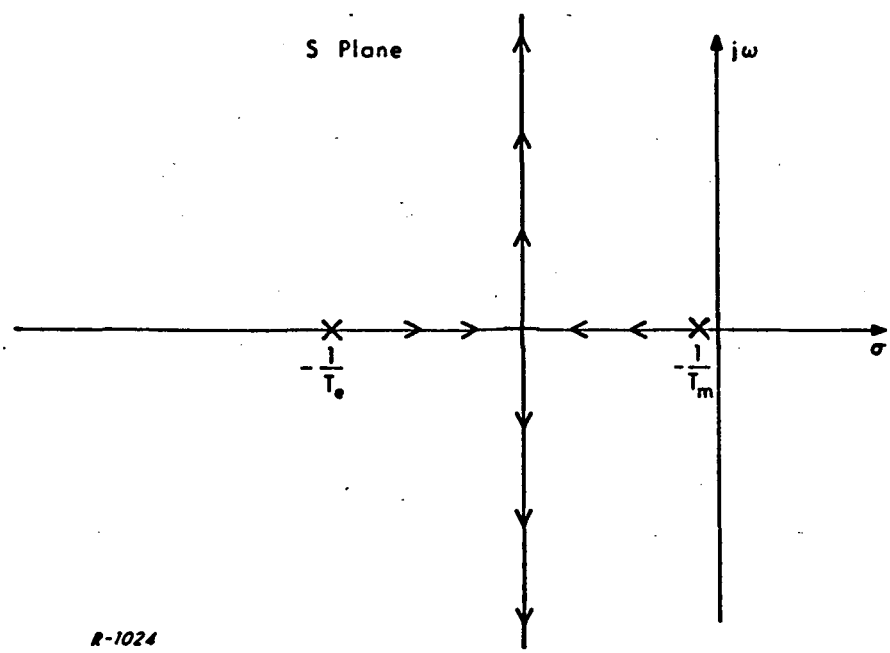

Fig. 14 Root-Locus Plot of the Open Loop Transference of the Minor Loop.

two roots at $1/T_e$ and $1/T_m$ move toward each other then become complex, traveling equidistantly along the line parallel to the $j\omega$ axis given by:

$$\sigma_o \approx \frac{T_m + T_e}{2T_m T_e} \tag{26}$$

Thus the transference $E_o(s)/E_{in}(s)$ is dominated by a pair of relatively-resonant complex poles. If T_e is small enough, then $\sigma_o \approx 1/2T_e$, and the value of T_m is not particularly important.

Now, the design objectives are a wide closed-loop bandwidth, relatively flat lowpass response, and high loop gain in order to reduce motor stiction. Flat response is achieved by increasing σ_o to move the poles away from the $j\omega$ axis and reduce the resonance peak. Thus we should strive for the smallest T_e possible. The bandwidth is increased by increasing loop gain to move the poles further away from the σ axis. However, if the poles are moved too far away from the σ axis then the response will begin to exhibit a resonance peak which detracts from the flatness. Thus the choice of loop gain is clearly a compromise between bandwidth and flat response.

There are further difficulties preventing the choice of large loop gain. The presence of additional time constants not shown in the model of Fig. 13 - such as amplifier poles - will make the root loci bend toward the $j\omega$ axis as the gain is increased, so that the loop will eventually become unstable. In addition, if the gain is increased to widen the bandwidth at the cost of an appreciable resonance peak, new problems are caused by brush-noise generation in the tachometer. This noise is a result of the self-magnetizing current of the tachometer, and appears even when the tachometer output is very lightly loaded. When the motor runs at a moderate speed, the brush-noise has sufficient components in the resonance-frequency region that the minor loop saturates and becomes unstable. The net effect of this brush-noise is to restrict the maximum permissible motor speed for a given loop gain.

The previous remarks are based on actual experience obtained during system development. The lowest achieved T_e was 1.6 ms. It was possible to increase the minor loop gain until K_3K_4 shown in Figs. 12 and 13 reached 150 before instability occurred. The resulting closed-loop bandwidth was about 300 Hz, with a 12 dB resonance peak near band-edge. It was possible by increasing the bias voltage to increase the motor speed until the brush-noise components fell near resonance resulting in saturation and instability. The stiction was reduced by the gain factor of 150, which is not enough for satisfactory system operation.

The solution to this dilemma was found to be equalization. An RC network was inserted across the summing amplifier in such a way as to create a zero in the open-loop transference exactly superimposed on the pole at $-1/T_e$. The root locus of the remaining pole thus became the negative σ axis, and the complex poles with their resonance problems were completely eliminated. Now the loop gain can be greatly increased before instability takes place, and the brush noise no longer severely limits the dynamic range of the loop nor the maximum permissible motor speed. A gain K_3K_4 of 1000 was achieved, with a closed-loop bandwidth of about 500 Hz. This in turn reduced the effective stiction by a factor of 1000 to an acceptable level. It is noteworthy that the instability occurring when this gain exceeds 1000 is still due to additional time constants not included in the linear model.

The resulting transference replacing Eq. (24) is readily shown to be

$$\frac{E_o(s)}{E_{in}(s)} = \frac{\alpha K_2 K_3 K_4}{\alpha K_2 K_3 K_4 + 1 + T_m s} \tag{27}$$

The transference from $e_o(t)$ to the shaft rotation $\psi(t)$ is simply $1/T(s)$, so that the minor-loop transference from input to shaft rotation output is

$$\frac{\Psi(s)}{E_{in}(s)} = \frac{E_o(s)}{E_{in}(s)\,T(s)} = \frac{K_2 K_3 K_4}{s(\alpha K_2 K_3 K_4 + 1 + T_m s)} \tag{28}$$

The closed minor-loop gain, corresponding to β of Fig. 11 and given approximately $1/\alpha$, was adjusted to unity by manually adjusting the tachometer gain α. The transference of Eq. (28) is then very closely approximated by

$$\frac{\Psi(s)}{E_{in}(s)} \approx \frac{1}{s\left(1+\frac{T_m}{\alpha K_2 K_3 K_4}\, s\right)} \tag{29}$$

An s-plane plot of the transference of Eq. (29) is shown in Fig. 15. The pole at the origin is the desired pole to fit the model of Fig. 11. The pole due to the mechanical time constant T_m has been moved away along the negative σ axis, until the bandwidth of the minor loop reaches about 500 Hz. This pole represents the failure of the minor loop to achieve the perfect integrator characteristic required to fit the ideal model of Fig. 11.

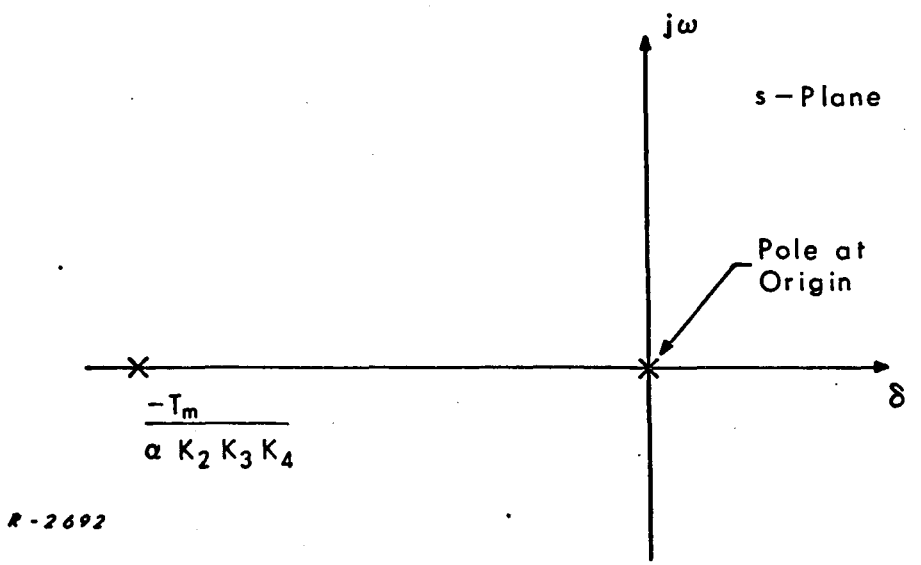

Fig. 15 S-Plane Plot of the Minor-Loop Transference, After Compensation.

3.3 Analysis and Design of the Actual Loop

We have indicated in Sec. 2.3 that the automatic-detection loop bandwidth is selectable in 5 dB steps of 0.16, 0.5, 1.6, 5, and 16 Hz. This greatly facilitates spectral analysis of a large class of oscillators. Most 5th overtone crystal standards have a break in their $S_{\dot{\phi}}(\omega)$ characteristic such that external additive noise effects are usually dominant as ω increases from this point. Thus, $\omega_c = 2\pi$ represents a commonly occurring point for transfer from direct $S_{\Delta\phi}(\omega)$ measurement to direct $S_{\Delta\dot{\phi}}(\omega)$ measurement. In all likelihood, measurements of weaker atomic resonance oscillation should be crossed over at a lower ω_c, while crystal oscillators driven harder than 5th overtone standards will require larger ω_c.

It should be pointed out that one does not normally desire to take $S_{\Delta\phi}(\omega)$ and $S_{\Delta\dot{\phi}}(\omega)$ data using the same ω_c, such that the resulting spectra have been passed through complementary Butterworth filter functions. On the contrary, one is far more likely to measure $S_{\Delta\phi}(\omega)$ data extending to an ω_c much lower than the similar upper limit of $S_{\Delta\dot{\phi}}(\omega)$ data. This gives an overlapping region where spectral data has been obtained from both outputs, such that there is an opportunity to check the ω^2 theoretical relationship between spectra. This allows a considerable relaxation of the "flatness" requirement of the $\Delta\phi(t)$ output, which is limited by the bandwidth of the minor loop, in that the smaller selections of ω_c will normally be in effect when this output is being observed.

The basic design equations for the loop are given in Eqs. (15) through (17). In order to achieve low residual phase errors and large lock range, it is necessary to choose a large loop gain $K_1\beta$. Equation (15) shows that the time constant T_2 must be correspondingly large to achieve small loop bandwidths ω_c. This presents two problems. First, when the loop is unlocked and attempting to acquire, the circuit acts essentially as an open-loop system

charging up with time constant T_2. It is clear that unaided acquisition could take hours, so manual acquisition aiding by adjusting the bias voltage may be required. Second, the synthesis of T_2 with passive elements would require extremely large capacitors. We resort to active-synthesis techniques described in the Appendix to synthesize the loop filter.

A circuit diagram of the loop filter synthesis is shown in Fig. 16. The component values are chosen according to Eqs. (15) through (17) so that the ideal loop represented by Fig. 11 has the desired Butterworth closed-loop characteristics mentioned in Sec. 3.1. The switching strategy is to establish the appropriate T_1 and T_2 for any ω_c while maintaining the loop gain constant. This is accomplished by switching R_2 and C_2 together via switch S3. R_1, R_3, R_4, and R_5 of Fig. 16 fix the dc gain of the active filter, hence these components are not changed.

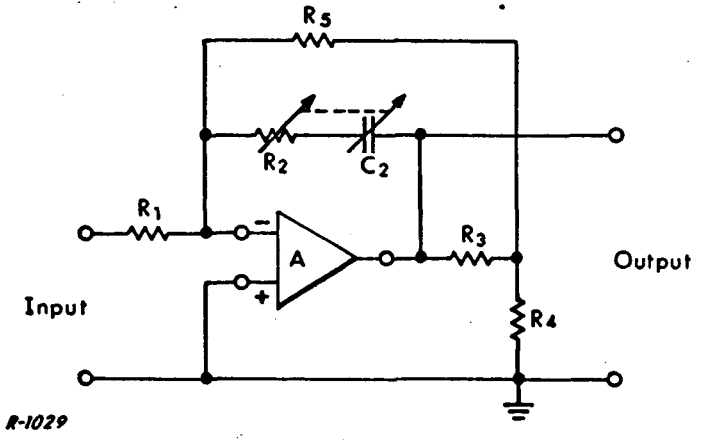

Fig. 16 Active Synthesis of the Loop Filter.

Since the minor-loop transference, given in Eq. (29), represented an imperfect integrator, we expect that the transferences of the actual automatic-detection loop to be only approximations of the desired Butterworth characteristics. Utilizing Eq. (29) and Fig. 11, we can write the two closed-loop transferences as

$$\frac{X(s)}{V(s)} = \frac{s\left(1+\frac{T_m s}{\alpha K_2 K_3 K_4}\right)\left(1+T_2 s\right)}{s\left(1+\frac{T_m s}{\alpha K_2 K_3 K_4}\right)\left(1+T_2 s\right)+K_1\left(1+T_1 s\right)} \tag{30}$$

and

$$\frac{Y(s)}{V(s)} = \frac{K_1 s\left(1+\frac{T_m s}{\alpha K_2 K_3 K_4}\right)}{s\left(1+\frac{T_m s}{\alpha K_2 K_3 K_4}\right)\left(1+T_2 s\right)+K_1\left(1+T_1 s\right)} \tag{31}$$

A comparison of these two transferences and the corresponding transferences of the ideal loop (Eqs. (13) and (14)) shows that the undesired pole in the minor loop gives rise to an extra zero at its undesired poles s-plane location, and to an extra pole on the negative σ-axis. Thus the location of the two complex poles and the one real pole is determined by the gain K_1 and the location of the undesired minor-loop pole ($-T_m/\alpha K_2 K_3 K_4$). The design procedure is then to attempt to bring the two complex poles as close as possible to their ideal Butterworth locations, and to keep the real pole as far away as possible from the origin to maintain flat inband response.

Several root-locus plots were made before finally choosing a value for gain K_1. The final choice was a compromise that resulted in fairly flat response for the low bandwidth settings (0.16, 0.5 and 1.6 Hz), and somewhat resonant responses for the high settings (5 and 16 Hz). At these high settings the two complex poles approach the $j\omega$-axis resulting in perceptible resonance peaks. This accounts for the occasional instability at the 16 Hz setting mentioned in Sec. 2.3.

4. ANALYSIS AND DESIGN OF THE ERROR MULTIPLIER

4.1 Error Multiplier Operation

An error multiplier has been developed as a predetection block to increase the sensitivity of the measurement system. A block diagram of a general n-stage error multiplier is shown in Fig. 17. The square blocks in Fig. 17 represent frequency multipliers with their multiplication factors written inside the blocks. The two original, independent, oscillator signals are the inputs $e_1(t)$ and $e_2(t)$ shown in Fig. 17 when the error multiplier is used. It is assumed that the mixer blocks contain bandpass filtering such that only the difference frequencies (and the associated spectral regions) are present at their outputs. The index i refers to the number of iterations of the basic scheme involved in any $e_a(t)$ output. Any of the outputs $f_i(t)$, where $1 \leq i \leq n$ and $e_2(t)$ are the two input signals to the automatic detection loop. The error multiplier actually implemented and depicted in Fig. 11 is a single-stage version of that shown in Fig. 17.

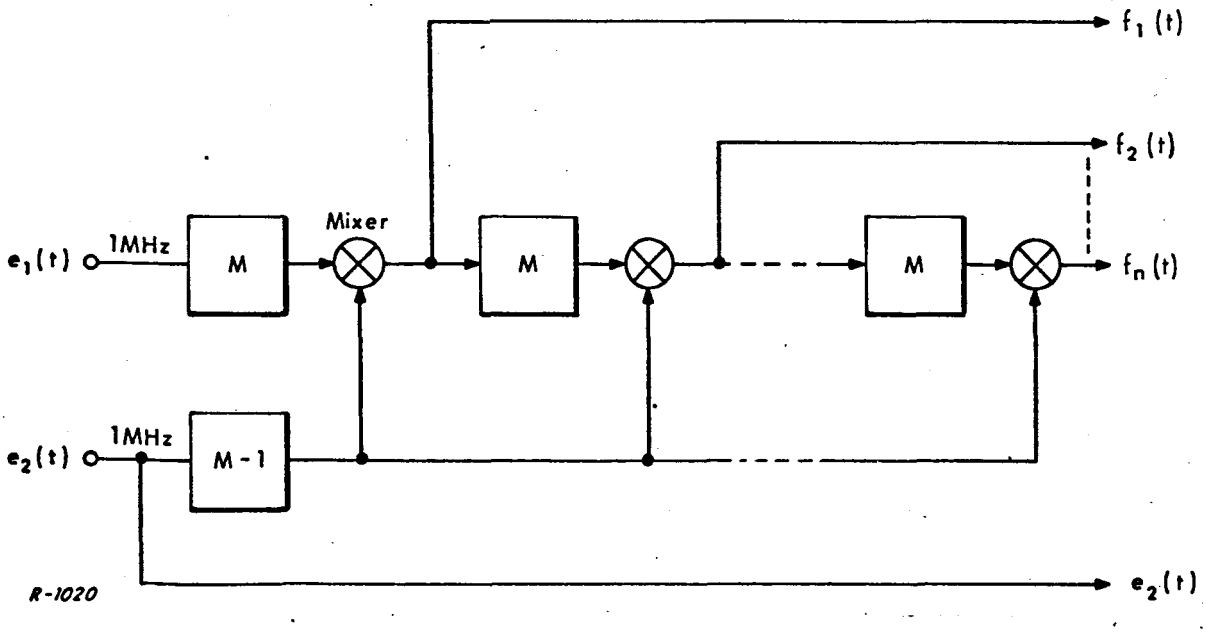

Fig. 17 Basic Block Diagram of an n-Stage Error Multiplier.

It has been shown in Sec. 4.4.3 of Ref. 1 that

$$e_{a_i}(t) = a_i(t) \cos\left[(M^i \Delta \bar{f} + \bar{f}_2)\, 2\pi t + M^i \Delta\phi(t) + \phi_2(t)\right] \tag{32}$$

The input to the linearized automatic-detection loop is then modified from Eq. (10) and Fig. 11 to

$$v_i(t) = A\left[2\pi M^i \Delta \bar{f} t + M^i \Delta\phi(t)\right] \tag{33}$$

It can be seen that the phase fluctuations have been amplified by the factor M^i, but so has the frequency offset $\Delta\bar{f}$. Thus, the motor is now required to rotate M^i times as fast when operating in conjunction with the error multiplier. It was also shown that the output spectra are given by

$$S_x(\omega) \approx A_1 \left\{ \frac{M^{2i}\omega^4}{\omega^4 + \omega_c^4} \left[S_{\phi_1}(\omega) + S_{\phi_2}(\omega)\right] + \left(\frac{2\pi M^i \Delta\bar{f}}{K_1 \beta}\right)^2 \delta(0) \right\} \tag{34}$$

and

$$S_y(\omega) = A_2 \left\{ \frac{(M^i/\beta)^2 \omega_c^4}{\omega^4 + \omega_c^4} \left[S_{\phi_1}(\omega) + S_{\phi_2}(\omega)\right] + \left(\frac{2\pi M^i \Delta\bar{f}}{\beta}\right)^2 \delta(0) \right\} \tag{35}$$

Here again, we see that the spectral densities have been magnified by a factor M^{2i}.

4.2 Error Multiplier Design Requirements

The error multiplier design must satisfy several requirements if it is to successfully enhance the oscillator fluctuations prior to detection. We formulate these requirements in this section, and discuss some of them in detail in the succeeding section.

In addition to multiplying the instantaneous phase or frequency, practical frequency multipliers attenuate and add noise to the incoming signal.

These effects limit the ultimate sensitivity of an error multiplier system employed to detect phase fluctuations of the input spectrum. If we assume that the "operating point" of the multiplier is set by the relatively large carrier component of the input signal, and consider the phase fluctuations to be small perturbations about this operating point, the error multiplier may be considered "linear" for these small fluctuations, and an analogy to the front end of a receiving system may be developed. Based on this front end analogy, and limited in validity by its qualifying assumptions, the basic design requirements of the error multiplier system may now be listed:

a) The overall multiplication factor M^i must be small enough so that the resultant peak phase deviation is much less than a radian, in order not to exceed the linear range of the phase detector characteristic or the dynamic range of the associated amplifiers.

b) The square of the multiplication factor must exceed the reciprocal of the insertion loss on a stage-by-stage basis if net phase-noise gain is to be assured. Thus, conversion efficiency of the multiplier is of paramount importance.

c) The equivalent input noise level of the error multiplier sets the ultimate sensitivity of the entire system. Hence, all stages, and especially the first few stages, must exhibit extremely low noise characteristics.

d) The bandwidth of the entire chain must be wide enough to pass the first order phase fluctuations of the input signal without distortion, and yet narrow enough to reject unwanted multiplier and mixer components.

The primary limitation on peak phase deviation in our system is the dynamic range of the amplifiers associated with the phase detector. Maximum permissible phase deviation is ± 0.1 radian, so that to ensure requirement (a) the product of M^i and the peak input phase deviation must not exceed this value. The phase output monitor M2 can be used to read the peak phase deviation with or without the error multiplier, then the multiplication factor can be chosen accordingly.

Passive multipliers (containing varactors) generally have low internal noise but high insertion loss, so that requirement (b) tends to set the upper limit on the total multiplication factor achievable. Active multipliers (containing transistors or vacuum tubes) generally have relatively high internal noise, so that requirement (c) tends to set the upper limit on the total multiplication factor achievable. The best multiplier design is chosen on the basis of desired input sensitivity and the actual sensitivity and dynamic range of the automatic-detection loop.

The ultimate requirements of an error multiplier to be used for measuring the characteristics of a specific oscillator are determined not only by the system characteristics, but also by the actual spectral densities and frequency offsets to be measured. Thus these requirements cannot be finally established until some preliminary measurements are performed on the oscillator using the existing measurement system. We have developed a 16-fold error multiplier using varactor doublers as building blocks, in order to demonstrate the general feasibility of the technique.

5. SYSTEM PERFORMANCE

5.1 System Sensitivity

The system sensitivity is determined by the residual noise spectral density at both the x(t) and y(t) outputs. Measurements of these residual spectra have been made by operating the system in common mode, i.e., by connecting the General Radio standard frequency oscillator to both the $e_1(t)$ and $e_2(t)$ inputs simultaneously. The results are presented in Figs. 18 and 19.

Figure 18 presents the residual phase-noise spectral density as abstracted from several independent measurements, with and without the error multiplier. Without the error multiplier, the residual noise is seen to be very low indeed. The discrete components at multiples of 60 Hz are obviously caused by power supply feedthrough. Their magnitudes were obtained by stopping the sweep on the Quan-Tech wave analyzer at the appropriate multiple of 60 Hz, then carefully taking a reading off the level meter incorporated in the wave analyzer to confirm the reading recorded by the X-Y plotter. It is useful to use this procedure in any measurement to isolate the discrete components.

The continuous part of the spectral density within the overall bandwidth limitation of the system is seen to have a slope of a 10 dB/decade, indicating the presence of f^{-1}-type noise, which is to be expected. The roll-off beyond 1.3 kHz is caused by the system bandwidth limitation.

The second curve in Fig. 18 shows the effect of the error multiplier on residual phase noise. The center portion of the continuous part of the spectral density has been raised about 20 dB, a consequence of the internal noise in the frequency doublers, mixer, and/or the amplifier incorporated in the error multiplier. Since the multiplication factor is 16 or 24 dB, the overall improvement in system sensitivity by the error multiplier is about 4 dB. Careful evaluation of the various sources of internal noise and redesign of the corresponding circuits should increase this improvement significantly.

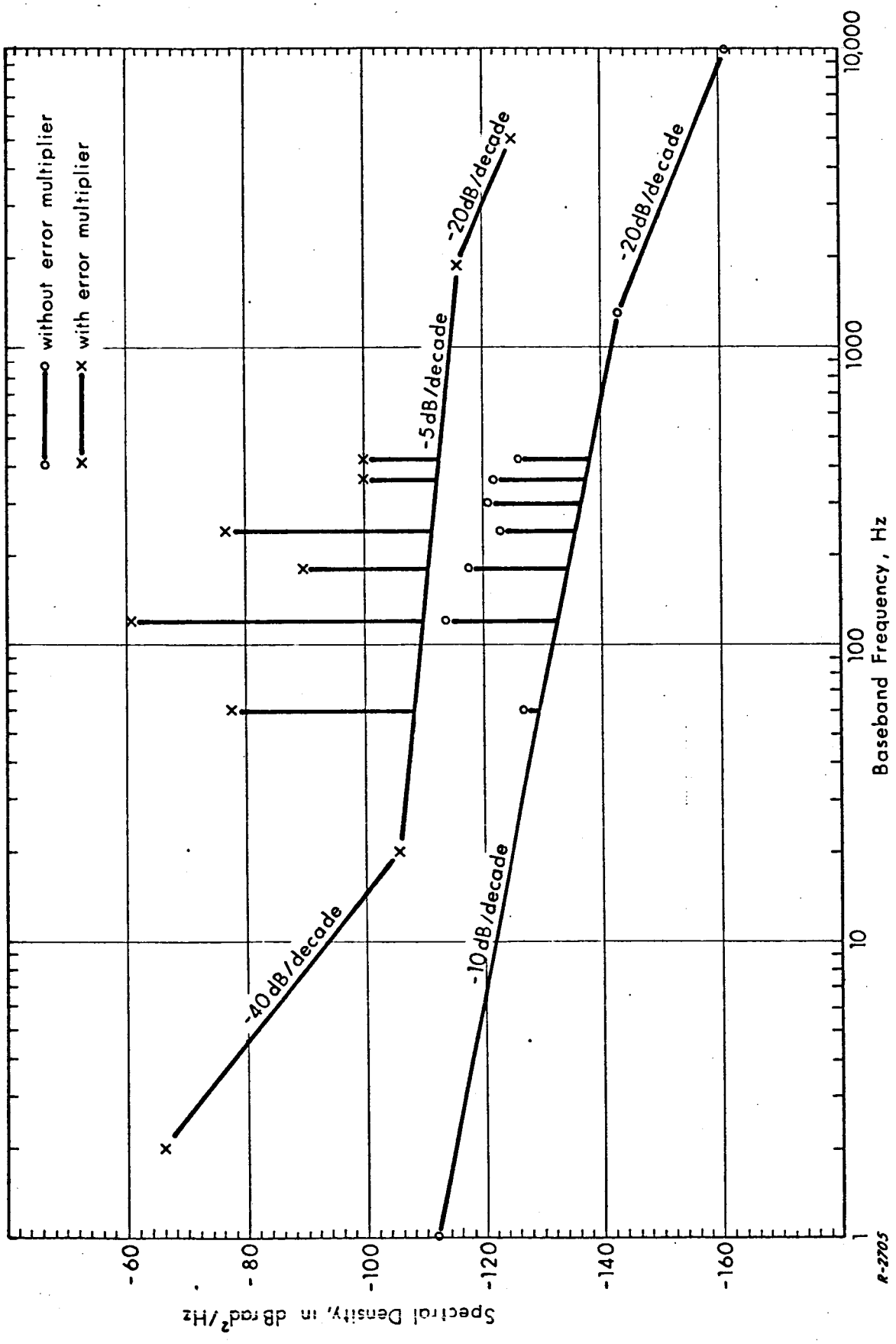

Fig. 18 Measured Residual Phase-Noise Spectral Density (ω_c = 1.6 Hz).

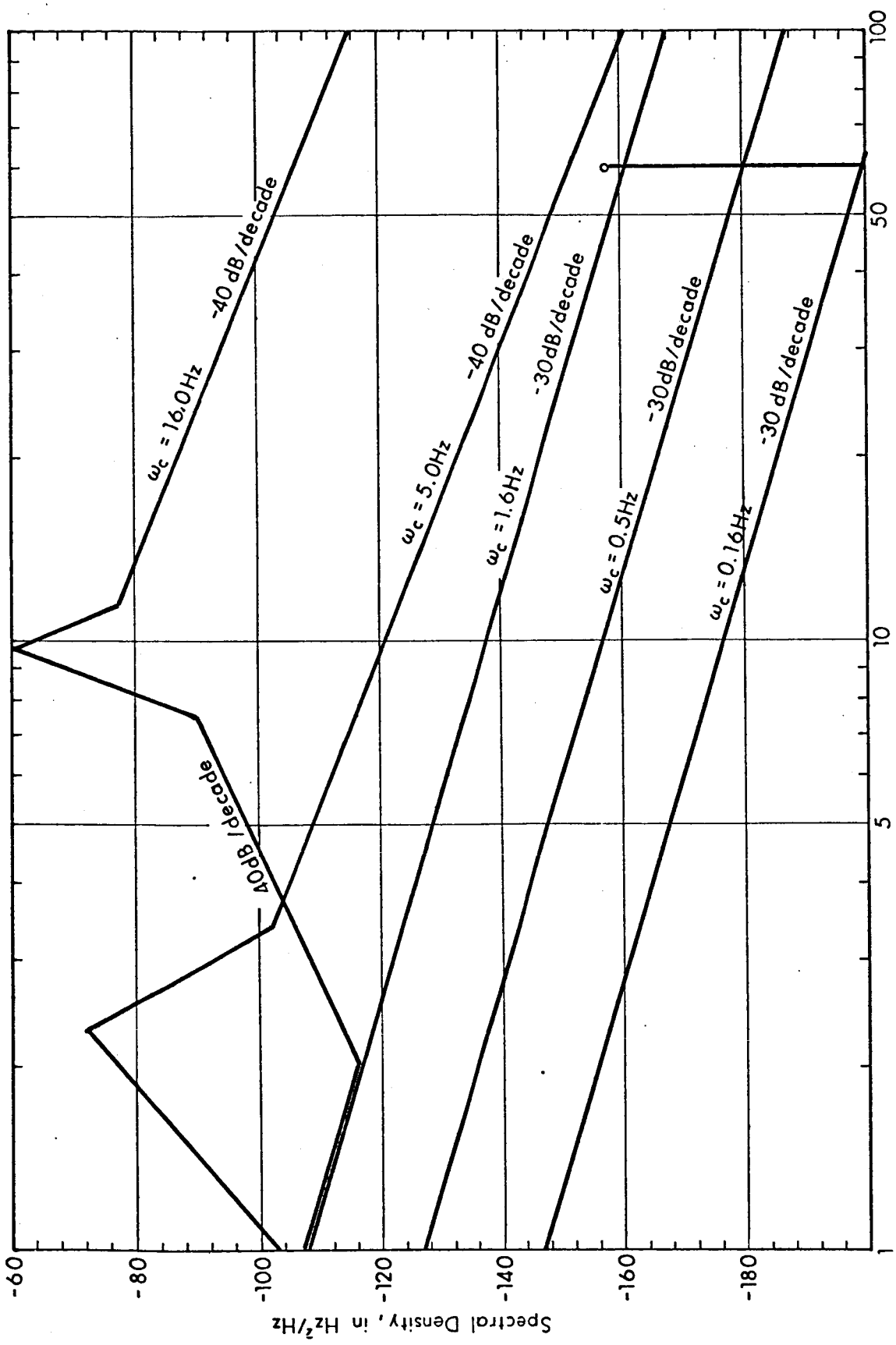

Fig. 19 Measured Residual Frequency-Noise Spectral Density.

The discrete components and the low-frequency portion of the continuous part of the spectral density are greatly increased by the error multiplier, probably because of power supply problems. It should be possible to reduce these effects by careful upgrading of the error multiplier design and components. Once these weaknesses in the error multiplier design are eliminated it will be possible to greatly increase system sensitivity by utilizing a multistage error multiplier, each stage resembling the existing multiplier.

Figure 19 presents the residual frequency-noise spectral density as abstracted from several independent measurements. Recall that the y(t) output was intended to be a Butterworth lowpassed version of the frequency fluctuations, so we expect a 40 dB/decade system skirt selectivity. Figure 19 shows 30 dB slope for the bandwidth choices ω_c = 0.16, 0.5, 1.6 Hz, thus confirming the presence of f-type frequency noise (equivalent to f^{-1}-type phase noise) which was observed in Fig. 18. The spectral densities corresponding to the bandwidths ω_c = 5 and 16 Hz exhibit the resonance phenomena mentioned in Sec. 3.3 above, and hence an undesired increase of the residual noise in the vicinity of the resonance frequencies. The 40 dB/decade skirt slopes would probably become 30 dB/decade if the resonances are removed, because the slopes indicated are too close to the resonance frequencies to be definitive.

5.2 System Operating Regions

The system is capable of yielding meaningful measurements of the fluctuations only when the input offset frequency and phase-fluctuation spectral density fall within certain limits. Figure 20 illustrates these limits.

The lower limit to the measurable spectral density is the residual phase-noise spectral density. This is indicated in Fig. 20 by horizontal lines corresponding to various baseband frequencies, as taken from Fig. 18. The upper limit is determined by the dynamic range of the phase detector and

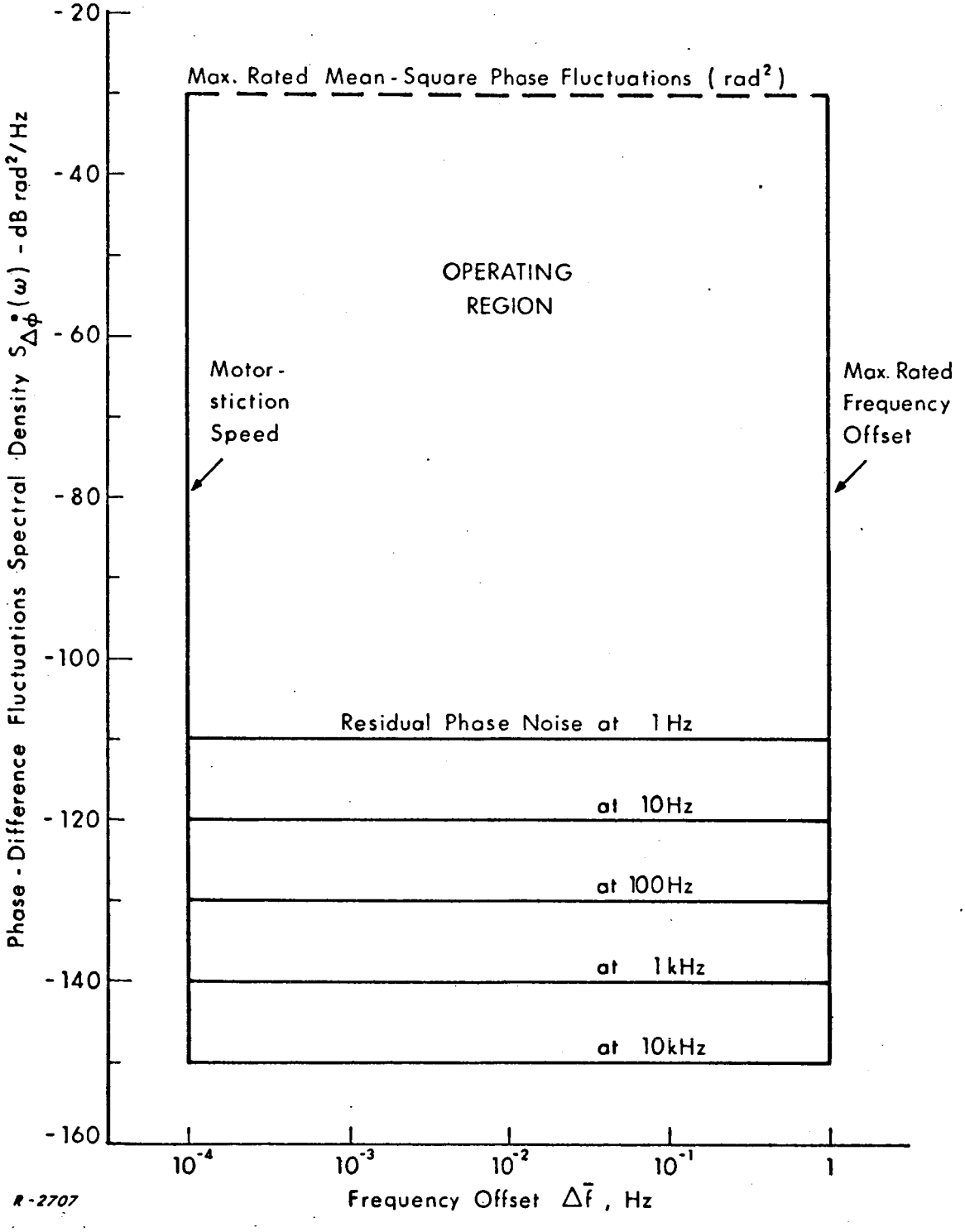

Fig. 20 System Operating Regions.

associated differential amplifier, which is ±0.1 radian peak. This limit is readily monitored on meter M2 with the aid of switch S1. Assuming a peak factor of 10 dB, the upper limit on mean-square phase fluctuation becomes 30 dB below one radian^2. This in turn sets an upper limit on the spectral density at any given frequency, but this limit is dependent on the actual shape of the spectral density. We pictorially indicate this limit in Fig. 20 by a horizontal dotted line at -30 dB, but the true upper limit on spectral density will be below this level.

The lower limit to the measurable frequency offset is determined by the stiction of the motor in the minor loop. This lower limit is 10^{-4}Hz, and it is indicated on Fig. 20 by a vertical line. Offset frequencies lower than this value would produce jerky rotation of the motor, thus resulting in unreliable data. The upper limit is determined by bearing friction and by the dynamic range of the power amplifier driving the motor. This upper limit is 1 Hz, and it is indicated on Fig. 20 by a vertical line.

Now we have in Fig. 20 a set of rectangles delineating the proper operating regions of the measurement system. In addition, we have on the next page a table summarizing the performance specifications of the system. If it is desired to measure the instabilities of an oscillator whose fluctuations lie below the lower boundaries of the rectangles indicated, then the error multiplier can be used to extend the region of operation to accommodate this oscillator. In that case, the multiplier will raise the lower limit on measurable phase fluctuations according to characteristics similar to Fig. 18, but in addition will raise the phase-fluctuation spectral densities themselves by a factor M^{2i}, and the frequency offsets by a factor M^i. When the various parameters are known, they should be checked against Fig. 20 to ensure that the resultant inputs to the automatic-detection loop fall within the operating regions.

SYSTEM PERFORMANCE SPECIFICATIONS

Input frequency	1.0 MHz ±1%
Input signal power	-13 to +17 dBm (0.05 to 1.6 volts) into 50 ohms
Input impedance	50 ohms ±20%
Maximum frequency offset between input signals	1 Hz (or 1×10^{-6} referred to 1 MHz)
Minimum measurable frequency offset	10^{-4} Hz (or 1×10^{-10} referred to 1 MHz)
Minimum measurable change in frequency offset (at low rates)	3×10^{-6} Hz (or 3×10^{-12} referred to 1 MHz)
Maximum measurable phase difference	0.1 radian peak (-20 dB referred to 1 radian)
Minimum measurable phase-difference spectral density	10^{-11} radians^2 per Hz at 1 Hz (-110 dB rad^2/Hz) decreasing at 10 dB per decade to 10^{-14} radians^2 (-140 dB rad^2/Hz) at 1 kHz
Phase difference x(t) output ranges	-40 to -100 dB rad per volt in 10 dB steps, -20 to -80 dB rad at 10 volts full scale on M2.
Frequency difference y(t) output ranges	10^{-5} to 10^{-1} Hz per volt in 1,2.5,5 steps, 10^{-4} to 1 Hz at 10 volts full scale on M3.
Frequency offset bias ranges	± 0.01, 0.1, 1 Hz full scale with 0-1000 vernier
Loop cutoff frequencies (ω_c)	0.16, 0.5, 1.6, 5, 16 Hz (1, 3.2, 10, 32, 100 radians/sec)

5.3 Some Typical Measurements

Figures 21 through 24 show some spectral density measurements on two typical oscillators, abstracted from many separate X-Y plots. The General Radio type 1115-B oscillator was always used as the reference $e_2(t)$. The phase and frequency spectral densities obtained for an oscillator incorporated in a CMC type 727B frequency counter are depicted in Figs. 21 and 22 respectively. The phase spectral density exhibits a 20 dB/decade continuous slope, and has substantial discrete components at multiples of 60 Hz. The frequency spectral density exhibits a flat portion within the loop bandwidth, which agrees with the 20 dB/decade slope observed in the phase spectral density.

The phase and frequency spectral densities obtained for an oscillator incorporated in an HP type 524C frequency counter are depicted in Figs. 23 and 24 respectively. The phase spectral density exhibits three different slopes as shown, and there is a rather broad discrete-like component at 320 Hz. The frequency spectral density exhibits a 10 dB/decade positive slope within the loop bandwidth. In order to agree with the corresponding slope in the phase spectral density, the latter should be -10 dB/decade instead of the -15 dB/decade shown in Fig. 23. The error is either instrumental, or in the graphical abstraction process to which the actual X-Y plots have been subjected.

To illustrate the graphical abstraction process, we include as Fig. 25 one of the actual X-Y plots from which Fig. 23 was abstracted. Note the possibility of error involved in drawing a best-fit straight line. Note also the trace at 60 Hz, where the magnitude of the discrete component was recorded after completing the sweep by returning the pen to the 60 Hz location and waiting for all transients to die down.

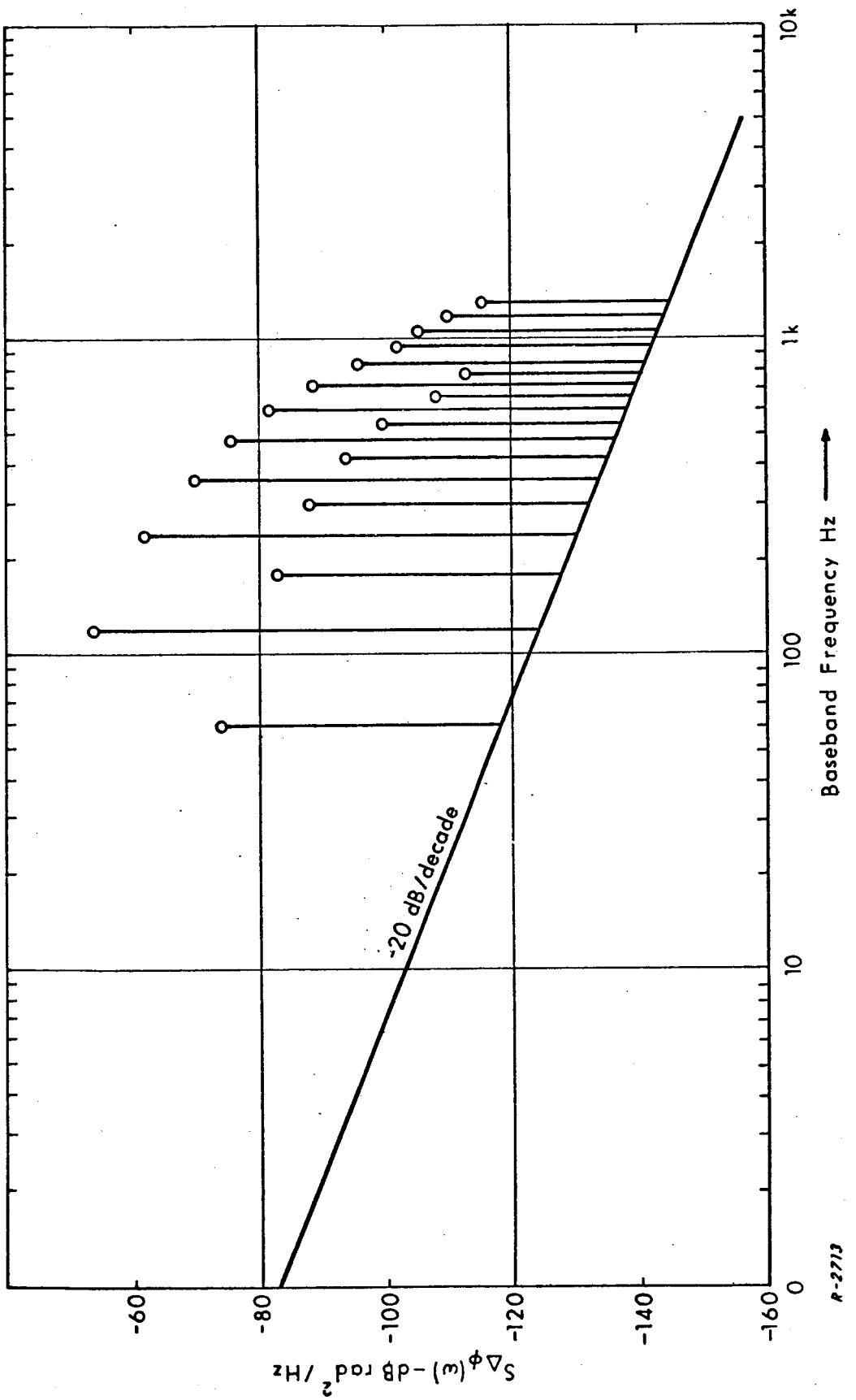

Fig. 21 Measured Phase-Difference Spectral Density, Oscillator from CMC 727B.

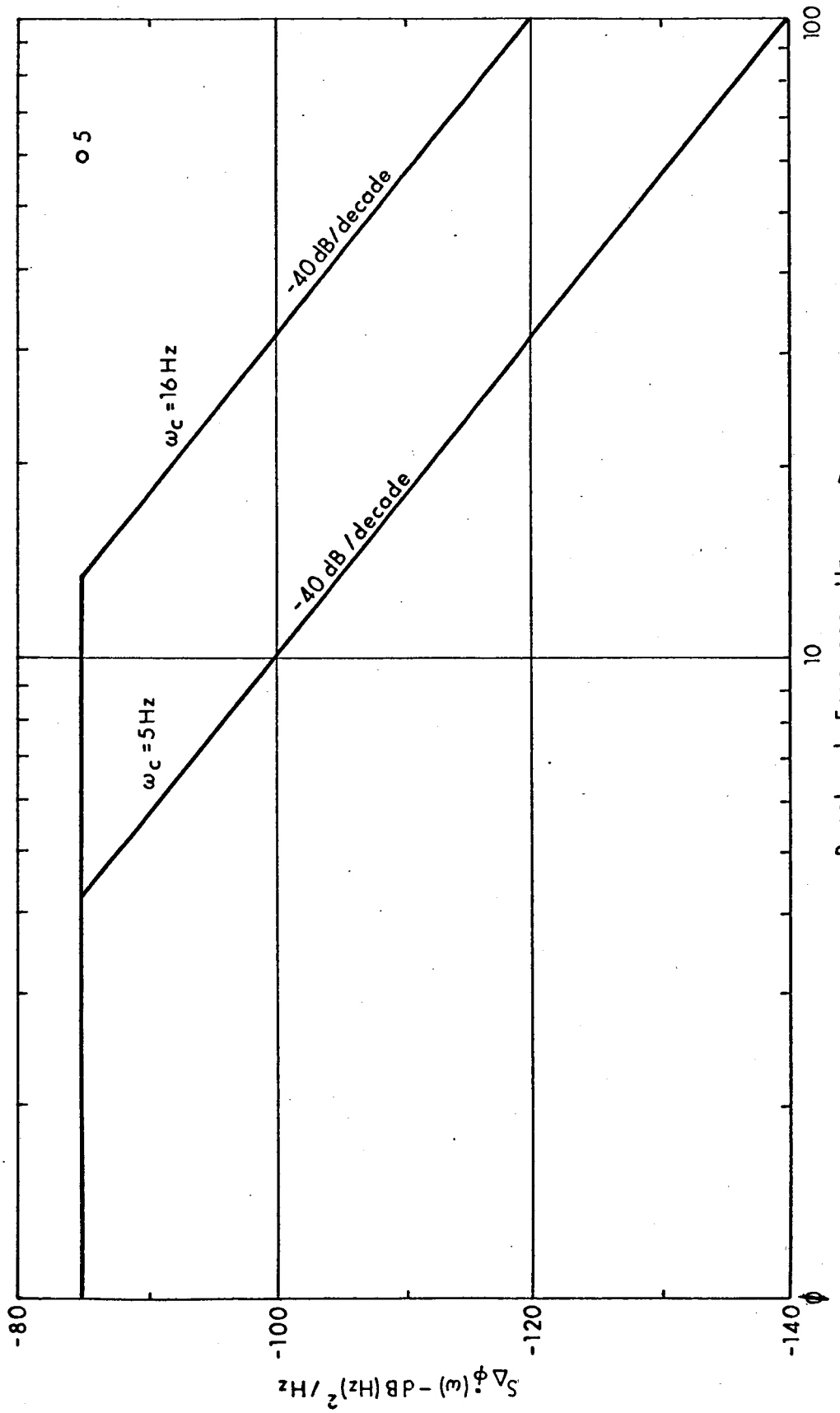

Fig. 22 Measured Frequency-Difference Spectral Density, Oscillator from CMC 727B.

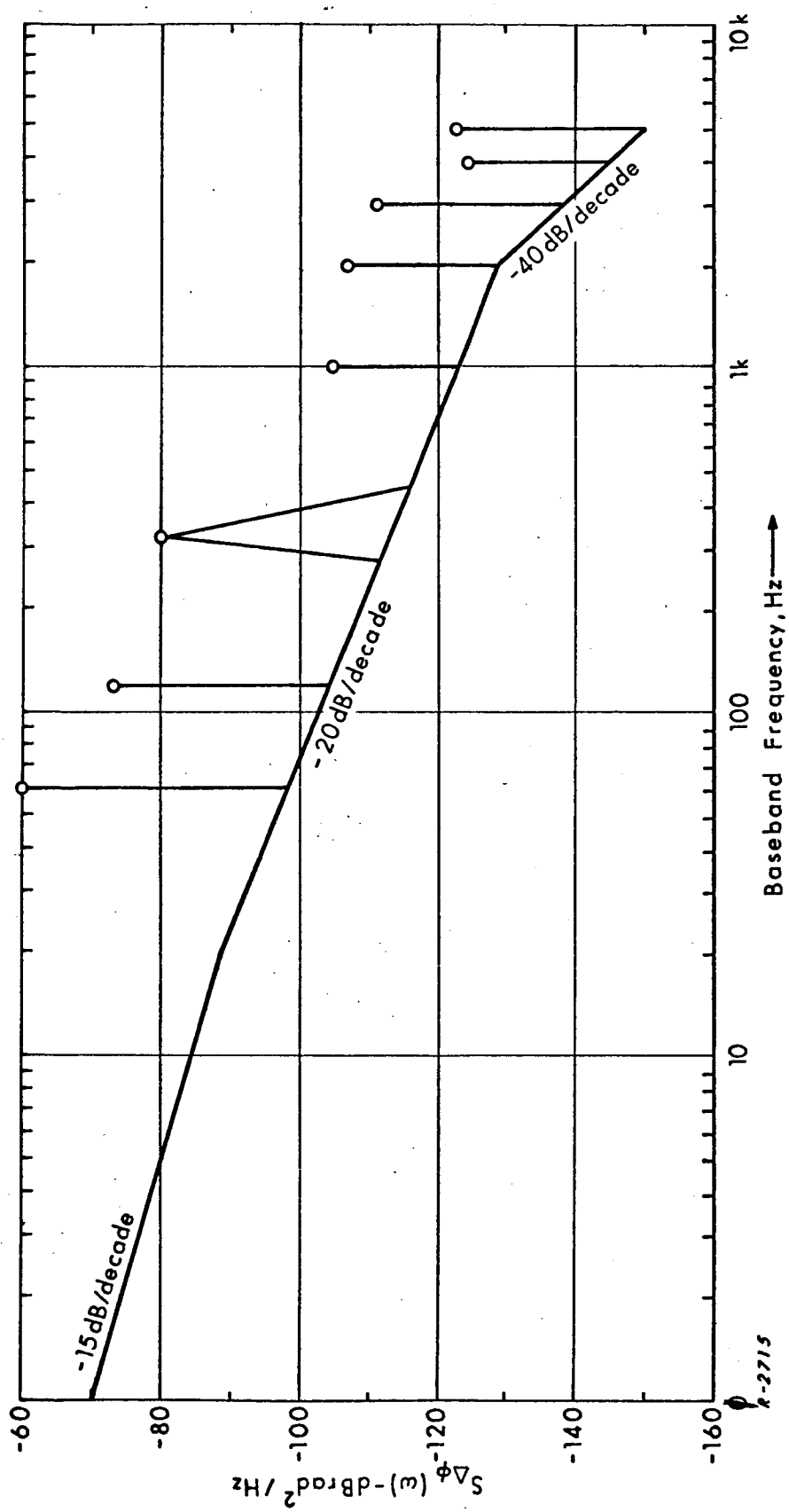

Fig. 23 Measured Phase-Difference Spectral Density, Oscillator from HP 524C.

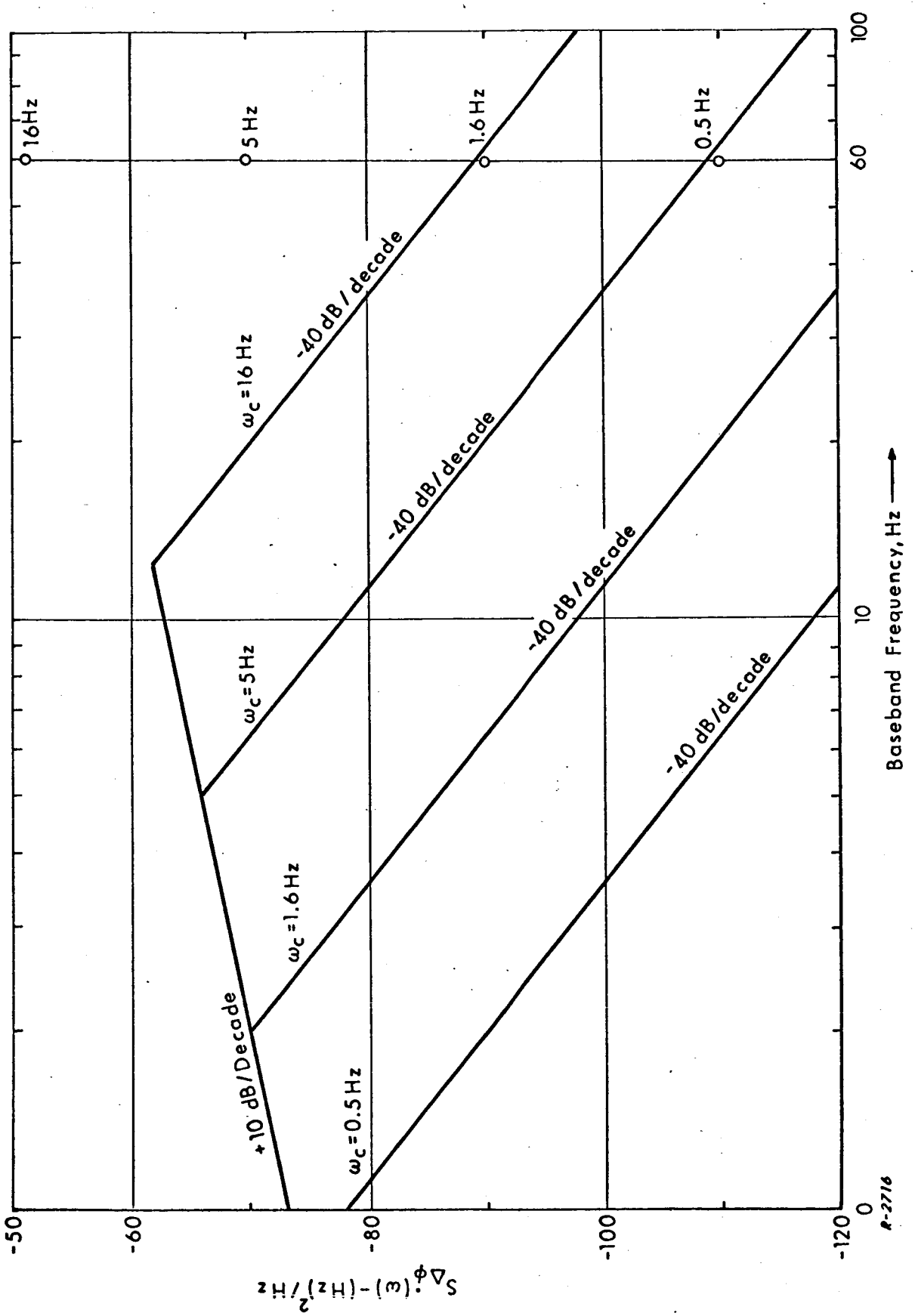

Fig. 24 Measured Frequency-Difference Spectral Density, Oscillator from HP 524C.

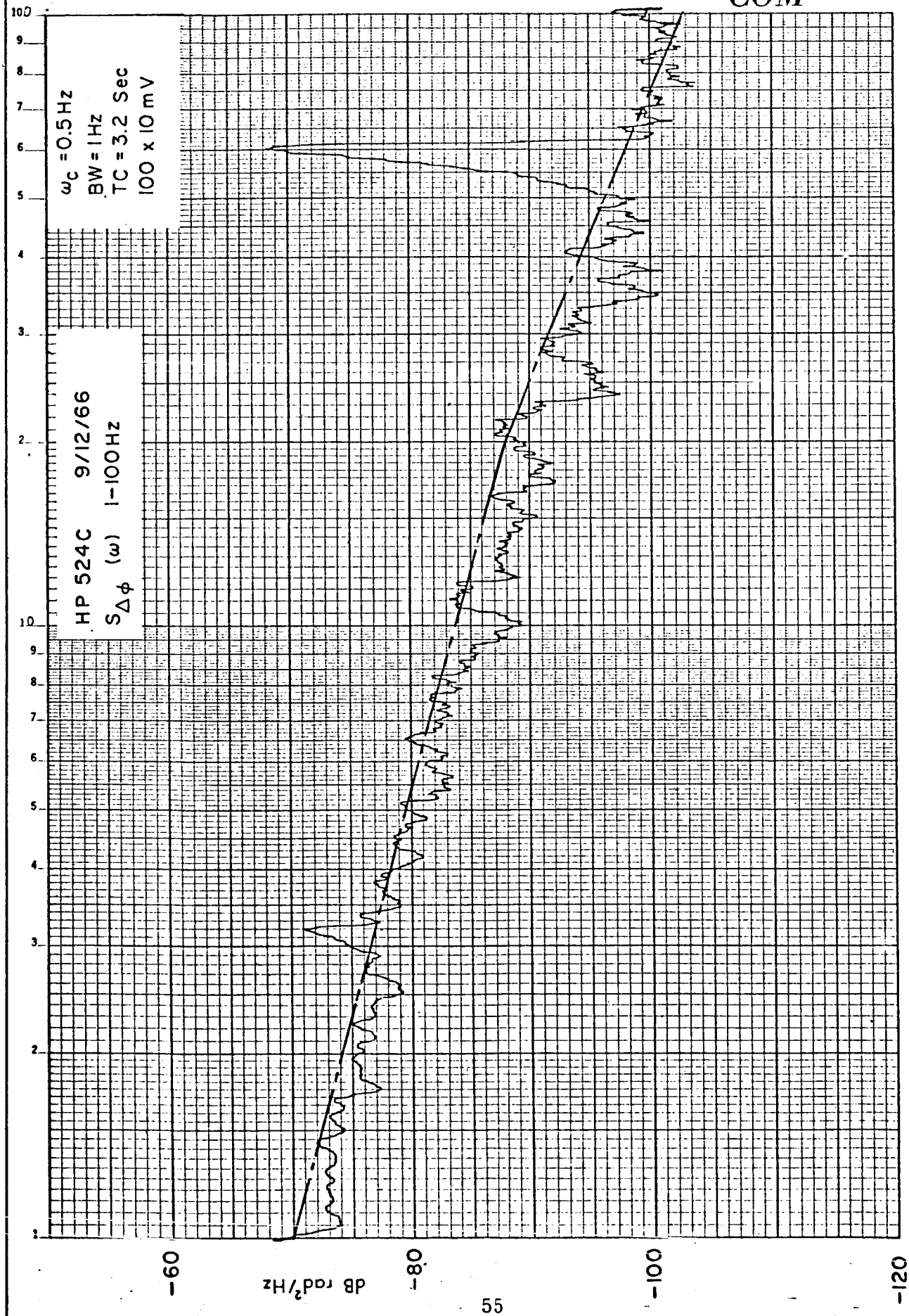

Fig. 25 Typical X-Y Plot, Corresponding to Portions of Fig. 23.

Several improvements can be suggested for inclusion in an advanced succdssor to the measurement system.

Two obvious improvements would be to reduce the brush-noise in the minor loop, and to decrease T_e such that a larger minor loop bandwidth could be maintained with less intrinsic resonance (see Sec. 3.2). Both improvements can be implemented simultaneously by employing printed-armature techniques in both the motor and tach. This printed armature rotating machinery has a more or less distributed armature such that discrete interruptions of current in a given armature winding are reduced considerably. Thus brush-noise generation is suppressed. The armature blocked-rotor equivalent circuit is a series impedance of a few microhenries of inductance and a few tenths of ohms of resistance. If motor armature of this type is fed from a relatively high resistance (current) source, the electrical time constant can be made vanishingly small. The problem in this would be to obtain sufficiently widebanc dc coupled current-mode power amplifiers that are short-circuit stable and have adequate current output. It is expected the industry will soon be able to supply coupled printed-armature motor-tach combinations whose brushes are so phased as to cancel brush-noise at the tach output. The cost of these devices for a given stiction speed, dynamic range, and maximum torque output is expected to be below that of comparable conventionally-wound devices.

Another worthwhile improvement would be to relocate the closed-loop poles in the system to eliminate the resonance at the bandwidth settings $\omega_c = 5$ and 16 Hz. Compensation networks other than those mentioned in Sec. 3.3 should be considered, as well as other loop filter functions based on the techniques of the Appendix.

Better components in place of some used in the present system can be used to improve system performance. DC amplifiers with dc drift corresponding to less than one-tenth the motor-stiction voltage would be a great

improvement. It would be worthwhile to investigate other types of resolvers which are compatible with the basic frequency offset requirements. Better regulated power supplies could probably reduce the residual noise in both the automatic-detection loop and the error multiplier. In particular, the discrete components at multiples of 60 Hz could be greatly reduced.

Other sources of residual noise, again in both the automatic-detection loop and the error multiplier, should be identified and evaluated, and methods devised to reduce their effects.

We should mention in closing that it would be very easy to design and fabricate a greatly simplified version of the measurement system intended solely for observing the slow drift fluctuations of $\Delta\bar{f}$. Such a system would be of particular value in evaluating unsynchronized time standards.

REFERENCES

1. ADCOM, Inc., "Theory, Characterization, and Measurement of Short-Term Frequency Stability with Application to Frequency Synthesis," Final Report, Task No. ASTR-AD-2, Contract No. NAS 8-11228, NASA report for George C. Marshall Space Flight Center, Huntsville, Alabama, 31 December 1964.

2. Baghdady, E. J., Lincoln, R. N. and Nelin, B. D., "Short-Term Frequency stability: Characterization, Theory, and Measurement," Paper presented at the Symposium on the Definition and Measurement of Short-Term Frequency Stability, held at Goddard Space Flight Center, 23-24 November 1964.

3. Baghdady, E. J., Lincoln, R. N. and Nelin, B. D., "Short-Term Frequency Stability: Characterization, Theory And Measurement," Proc. IEEE, Vol. 53, No. 7, pp. 704-722, July 1965.

4. Baghdady, E. J., Lincoln, R. N., Mullen, J. A. and Nelin, B. D., "Short-Term Frequency Stability," Proc. IEEE, Vol. 53, No. 12, p. 2110, December 1965.

5. Blackman, R. B. and Tukey, J. W., The Measurement of Power Spectra, Dover Publications, Inc., 1959.

APPENDIX

ACTIVE SYNTHESIS OF LOOP FILTERS

We desire to synthesize a transference

$$H(s) = \frac{-K_3(1+T_1 s)}{1+T_2 s} \tag{A-1}$$

where

$$T_2 > T_1 \tag{A-2}$$

and K_3 is a feedback-stabilized dc gain. An operational amplifier circuit is indicated in light of the large values of T_2 required. We shall develop a general method for analyzing operational amplifier circuits, and then use this method to analyze a particular circuit that satisfies Eq. (A-1) and derive design equations for the circuit.

Figure A-1 shows the general model of an operational amplifier circuit. N_1 and N_2 are linear, lumped parameter, passive, and bilateral networks. If we may consider the output impedance of the amplifier sufficiently small as to be negligible, then it is obvious that there is no feedforward path from V_{in} to V_{out} in Fig. A-1 other than through the input to output transference of the amplifier. Under this assumption, an equivalent model of Fig. A-1 can be drawn as shown in Fig. A-2, justified by the principle of superposition. It is important to realize that both B_1 and B_2 of Fig. A-2 are transferences in the linear, lumped, passive and bilateral network shown in Fig. A-3, since B_1 and B_2 are independent of the amplifier. (The one exception to this could be the case where the input admittance of the amplifier is not negligible. Even so, this admittance, unless it is negative or nonlinear, could be included in N_1 and thus the model is still general.)

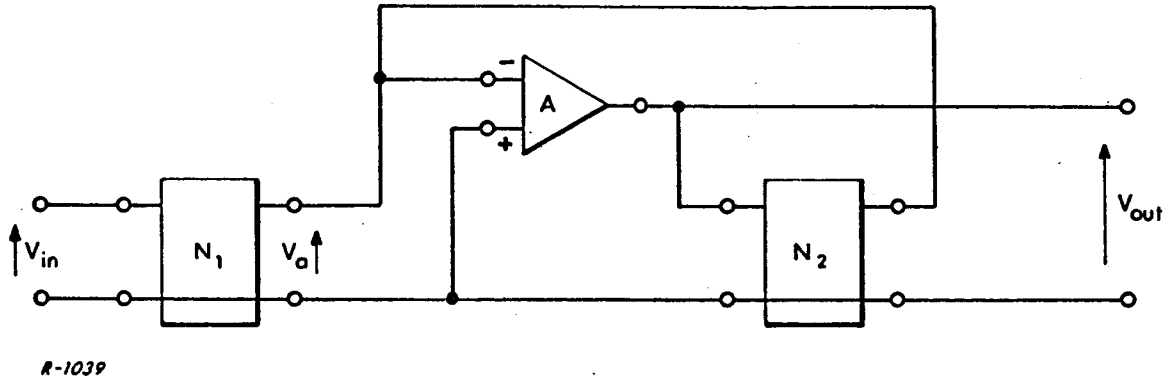

Figure A-1

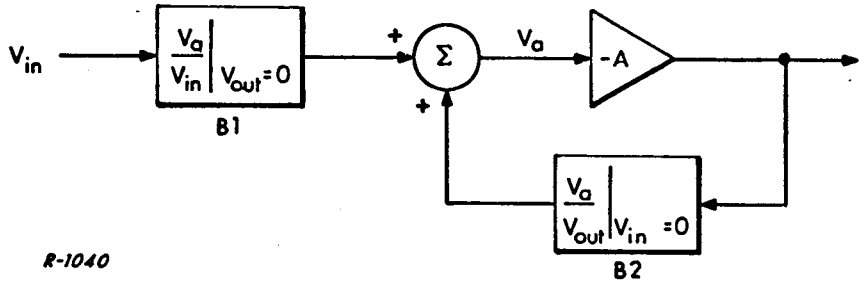

Figure A-2

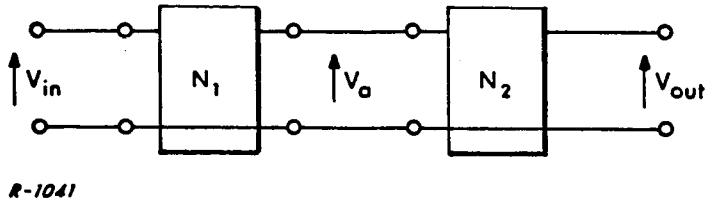

Figure A-3

As such, B_1 and B_2 can be written as ratios of polynomials of the Laplace variable, s, in the transform domain. It has been shown that the functions B_1 and B_2 as defined have the same denominator polynomial.* Thus we may write

$$B_1(s) = \frac{Z_1(s)}{P(s)} \tag{A-3}$$

and

$$B_2(s) = \frac{Z_2(s)}{P(s)} \tag{A-4}$$

where $Z_1(s)$ and $Z_2(s)$ are polynomials describing the "zeros" of their respective functions, and P(s) is a polynomial describing the "poles" common to both functions.

Applying elementary feedback theory to Fig. A-2, we may write

$$\frac{V_{out}(s)}{V_{in}(s)} = \frac{-AB_1(s)}{1 + AB_2(s)} \tag{A-5}$$

Substitution of Eqs. (A-3) and (A-4) yields

$$\frac{V_{out}(s)}{V_{in}(s)} = \frac{-AZ_1(s)}{P(s) + AZ_2(s)} \tag{A-6}$$

Equation (A-6) is the general relationship required to analyze any operational-amplifier circuit consistent with the feedforward assumption.

The particular circuit chosen to satisfy Eq. (A-1) is shown in Fig. A-4.

For this circuit

$$B_1(s) = \frac{\alpha(1 + sR_2C_2)}{1 + s(\alpha R_1 + R_2)C_2} \tag{A-7}$$

* Guilleman, E.A., Synthesis of Passive Networks, John Wiley & Sons, Inc., 1959.

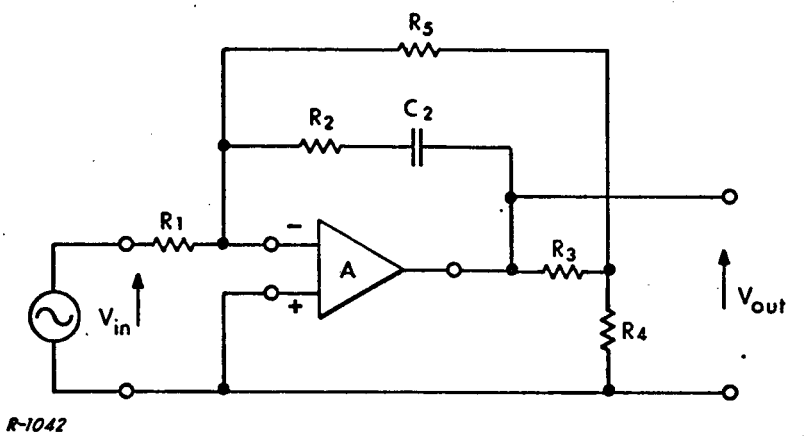

Figure A-4

and

$$B_2(s) = \frac{\beta + s(\alpha R_1 + \beta R_2)C_2}{1 + s(\alpha R_1 + R_2)C_2} \qquad \text{(A-8)}$$

where

$$\alpha = \frac{R_3R_4 + R_3R_5 + R_4R_5}{R_1R_3 + R_1R_4 + R_3R_4 + R_3R_5 + R_4R_5} \qquad \text{(A-9)}$$

and

$$\beta = \frac{R_1R_4}{R_1R_3 + R_1R_4 + R_3R_4 + R_3R_5 + R_4R_5} \qquad \text{(A-10)}$$

Substituting B_1 and B_2 into Eq. (A-6), we obtain

$$\frac{V_{out}(s)}{V_{in}(s)} = - \frac{\left(\frac{A\alpha}{1 + A\beta}\right)(1 + sR_2C_2)}{1 + s\left[\frac{\alpha R_1(1 + A)}{1 + A\beta} + R_2\right]C_2} \qquad \text{(A-11)}$$

Equation (A-11) can be seen to be of the correct form by comparing it to Eq. (A-1). Thus, we may equate (A-1) and (A-11) and identify obvious parts to obtain design equations.

$$-\frac{K_3(1+T_1 s)}{1+T_2 s} = -\frac{\frac{A\alpha}{1+A\beta}(1+sR_2C_2)}{1+s\left[\frac{\alpha R_1(1+A)}{1+A\beta}+R_2\right]C_2} \tag{A-12}$$

from which we obtain

$$K_3 = \frac{A\alpha}{1+A\beta} \tag{A-13}$$

$$R_2C_2 = T_1 \tag{A-14}$$

and

$$C_2R_1 = \frac{T_2 - T_1}{K_3 + \frac{K_3}{A}} \tag{A-15}$$

We may simplify the expressions for α and β if we let

$$\text{both } R_1 \text{ and } R_5 \gg \text{both } R_3 \text{ and } R_4 \tag{A-16}$$

Under these conditions

$$\alpha \approx \frac{R_5}{R_1 + R_5} \tag{A-17}$$

and

$$\beta \approx \frac{R_1R_4}{(R_1 + R_5)(R_3 + R_4)} \tag{A-18}$$

Equation (A-18) can be seen to be the transference of a cascade of two isolated voltage divider networks, indicating that the resistance of R_1 plus R_5 does not load the R_3, R_4 divider.

Thus we have shown that Fig. A-4 is a sufficient synthesis of Eq. (A-1). The design equations for the circuit may be summarized as

$$A = \frac{K_3}{\alpha - K_3\beta} \tag{A-19}$$

$$R_2C_2 = T_1 \tag{A-20}$$

$$R_1C_2 = \frac{T_2 - T_1}{K_3 + \frac{K_3}{A}} \tag{A-21}$$

and either

$$\alpha = \frac{R_5}{R_1 + R_5} \tag{A-22}$$

and

$$\beta = \frac{R_1R_4}{(R_1 + R_5)(R_3 + R_4)} \tag{A-23}$$

if condition (A-16) holds, or

$$\alpha = \frac{R_3R_4 + R_3R_5 + R_4R_5}{R_1R_3 + R_1R_4 + R_3R_4 + R_3R_5 + R_4R_5} \tag{A-24}$$

and

$$\beta = \frac{R_1R_4}{R_1R_3 + R_1R_4 + R_3R_4 + R_3R_5 + R_4R_5} \tag{A-25}$$

if condition (A-16) does not hold.

The stabilization of the dc gain can be calculated by differentiating Eq. (A-13) with respect to A, yielding

$$\frac{dK_3}{dA} = \frac{1}{(1 + A\beta)^2} \tag{A-26}$$

The assumption of negligible feedforward can be evaluated by considering the worst case when the input frequency is high enough that C_2 may be neglected.

The feedforward through the R_5 circuit plus the feed through the R_2 circuit (with C_2 shorted), both developed across the output impedance of the amplifier, must be negligible in comparison with the output of the amplifier at this frequency. This normal amplifier output is

$$\lim_{s \to \infty} H(s) = - \frac{K_3 T_1}{T_3} \qquad \text{(A-27)}$$